Antibodies and flow cytometric analysis

Anti-CD3-FITC, anti-CD4-allophycocyanin, anti-CD25-allophycocyanin, anti-CD44-phycoerythrin (PE), anti-CD62L-FITC, and anti-IL-17-PE were purchased from BD Biosciences (San Diego, CA). Anti-mouse Foxp3-PE (FJK-16S) was purchased from eBioscience (San Diego, CA). Anti-mouse CD3ε (clone 2C11) used for T cell stimulation and anti-mouse CD16/32 (clone 2.4G2) used for Fc receptor blocking were purified from hybridoma-cultured supernatants in our laboratory. Cells were incubated with antibodies for 30 min at 4°C and then washed to remove unbound antibodies. All the samples were analyzed with a FACSCalibur™ flow cytometer and the CellQuest™ program (BD Biosciences).

Preparation of lymphocyte culture and cytokine measurements

Single-cell suspensions were prepared from spleen and lungs of an 8 to 10 week-old mouse, in which the lung disease of interest is not developed. Lymphocytes in the lung were obtained by digesting minced lung tissues with 150 U/ml collagenase (Maeda Co. Ltd., Tokyo, Japan) as described previously [21]. The number of effector/memory and regulatory T cells were calculated based on the percentage of each subpopulation that was $CD44^{high}CD62L^{low}$ and $CD4^{+}Foxp3^{+}$, respectively, and the total cell number in each organ. Total lymphocytes isolated from lung tissues that contained equal number of effector/memory $CD4^{+}$T cells (normalized based on absolute number of effector/memory CD4 T cells) were stimulated with soluble anti-CD3ε (10 μg/ml) at 37°C for the indicated time. IL-13 levels were assayed in cultured supernatants using ELISA kit for IL-13 (R&D Systems, Minneapolis, MN), according to the manufacturer's recommendations. The production of IL-17 in lymphocytes was detected by intracellular staining with anti-IL-17-PE following incubation of lymphocytes for 4 h with 50 ng/ml PMA, 500 ng/ml Ionomycin (Sigma-Aldrich, St. Louis, MO) in the presence of 10 μg/ml brefeldin A (Invitrogen, Carlsbad, CA).

Genetic mapping

Genotypes of BCN2.TgL mice were determined by polymerase chain reaction (PCR) using genomic DNA prepared from the tail tip. The genotyping PCR was performed using standard reagent and the following conditions: 94°C for 5 min, 35 cycle of 94°C for 30 sec, 58°C for 30 sec, 72°C for 30 sec, and final extension 72°C for 5 min with the 98 microsatellite markers (additional file 1), which represent amplified fragment-length polymorphism between BALB and B6 strains. This genotyping provided full coverage of the mouse autosomes with the marker spaced an average of 12.5 cM apart and a maximum distance of 35 cM between any two markers. PCR products were visualized with electrophoresis on 2-4% agarose gels containing 0.01% ethidium bromide.

In a genome-wide scan, we determined genotypes of the 48 BCN2.TgL mice, which were selected as the top (severest) 24 and the bottom 24 on the list of PAH score, at all the 98 microsatellite positions (additional file 1) . The association at each microsatellite position was evaluated with chi-square test for independence between the genotypes and the two groups that were positive and negative for the incidence of PAH, using standard 2 × 2 contingency matrices. A p value less than 0.05 was regarded as suggestive association. The suggestive association was confirmed by the two-tail t-test for the difference of means between the two genotype groups of a total of 341 BCN2.TgL mice. In this test a P value less than 0.0034 was regarded as suggestive association. This P threshold was referred to the previous recommendation [22].

In a linkage mapping, a linkage position was determined with the quantitative trait locus (QTL) program. The logarithm of odd (LOD) was determined with the interval mapping program in the Windows QTL Cartographer (V2.5) software. The PAH scores of all BCN2.TgL mice were used as an indicator of phenotype. A suggestively significant level ($\alpha = 0.05$) of LOD was determined by the permutation test installed in this software (1000 permutations). Map positions (cM) of the microsatellite makers were based on the information of the Mouse Genome Database of The Jackson Laboratory (http://www.informatics.jax.org).

Statistics

A 95% confidence interval shown in Table 1 was calculated using the method described previously [23]. The two-tailed t-test was used to evaluate a difference of

Table 1 Summary of PAH scores of B6, BALB, and transgenic strains of mice

Mice*		n†	Median of score	95% CI‡	Statistics§
B6		9	0	0 - 0.1	
BALB		2	0	n.d.	
B6. TgL		15	0.7	0.35 - 1.05	¶
BALB. TgL		8	0	0 - 0.1	
BCF1. TgL		30	0.05	0 - 0.1	
BCN2. TgL	female	174	0.25	0.2 - 0.4	¶
BCN2. TgL	male	167	0.25	0.2 - 0.4	¶

* All mice were killed at 20 week-old for this examination. BCF1, BALB × B6; BCN2, BCF1 × B6.TgL.

† Number of mice tested.

‡ CI, confidential interval. The CI was not determined (n.d.) for BALB/c (BALB).

§ The significance of this study was evaluated by Mann-Whitney U-test for the all strains.

¶, P < 0.01 (v.s. B6).

means between two groups. A P value less than 0.05 considered as significant.

Results

Histopathological characterization of the lung phenotype

Microscopic examination revealed diffuse pathological changes in the small- to medium-sized pulmonary arteries in B6.TgL (Figure 1A, E), but not in B6 (Figure 1B), BALB strain of OX40L transgenic mice (BALB.TgL) (Figure 1C), or BALB (Figure 1D). This vascular lesion was found to be readily accompanied with perivascular infiltration of lymphocytes and, to a lesser extent, neutrophils (Figure 1F). These changes were mainly observed in arteries contained in bronchovascular bundles (respiratory arteries) and were typically characterized by fibrocellular endothelial proliferation of the intimal layer and, to a lesser extent, medial muscular hypertrophy (Figure 1G and 1H). Neither muscularization of distal pulmonary arterioles, which is a common pathological change in a hypoxic PAH model, nor plexiform lesions, found in human PAH, were identified. The cells in the intimal lesion were characterized as positive for a myofibroblast marker, smooth muscle-specific actin (αSMA) (Figure 1I), and an endothelial cell marker, CD31 (Figure 1J). When no treatment was administered to avoid vasospasm before the histopathological preparation, vasoconstriction was frequently observed in pulmonary arteries of B6.TgL but not in wild-type B6, BALB, and BALB.TgL mice, irrespective of the presence of the overt pathological changes mentioned above (data not shown). Perivascular lymphocytic infiltration was also observed around pulmonary veins; however, there was no pathologic remodeling in those veins as observed in the

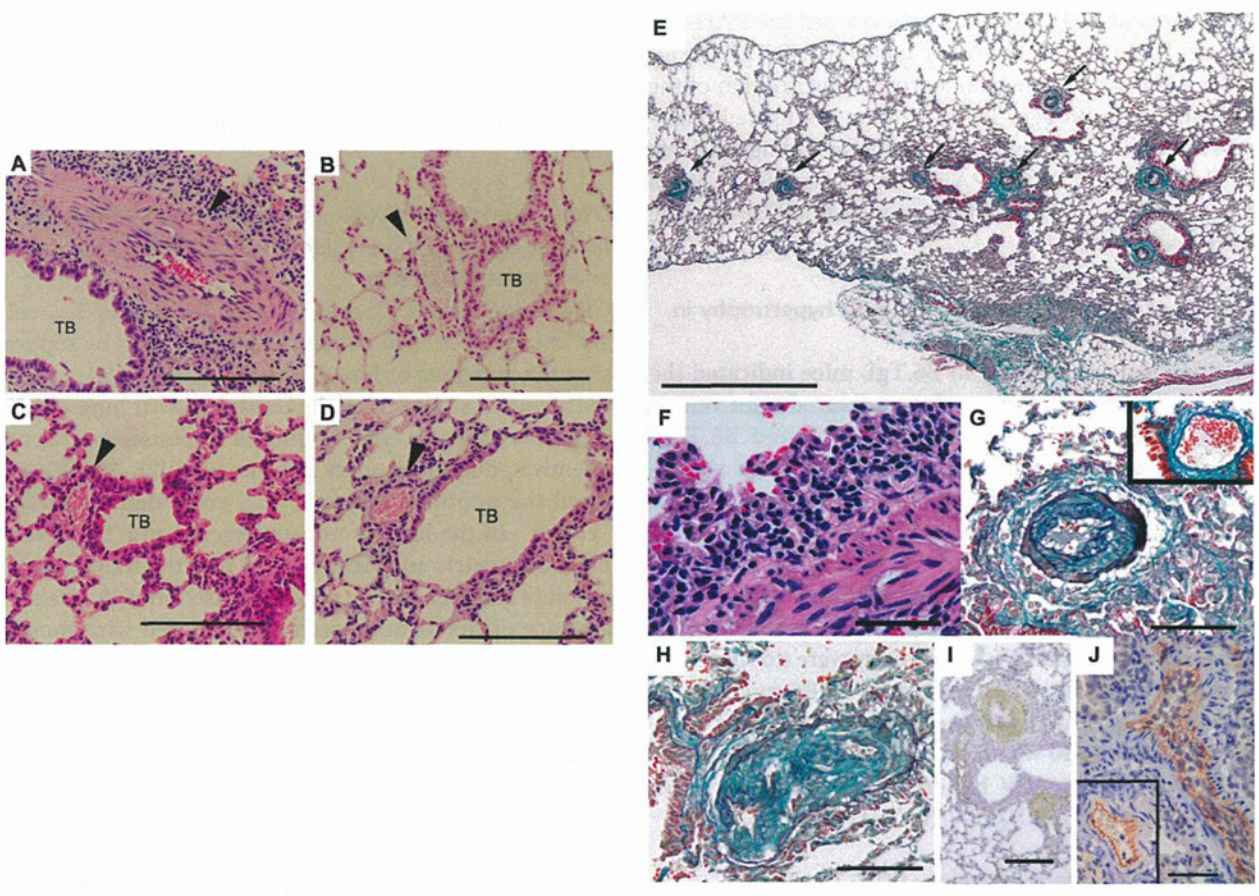

Figure 1 Histopathological features of the lung disease in B6. TgL mice. (A-D) Histopathological manifestation typically present in B6.TgL (A). No pathological manifestation observed in B6 (B), BALB.TgL (C), and BALB (D). The photograms indicated were taken from over 20-week aged male mouse. Arrow heads indicate pulmonary arteries. *TB*, terminal bronchiole. H&E staining. Scale bar = 100 μm. (E) Diffuse pathology present in B6.TgL. Masson's trichrome staining. Scale bar = 1 mm. (F) Perivascular lymphocytic infiltration in the affected lung. H&E staining. Scale bar = 50 μm. (G, H) Representative microscopic appearance in the affected arteries in the B6.TgL lung. An inset photogram in *G* represents the appearance of a normal pulmonary artery. Thickening of the intimal and, to a lesser extent, medial layers with marked intimal fibrosis is characteristic of the affected arteries. Masson's trichrome staining. Scale bar = 100 μm. *I* and *J*, expression of αSMA and CD31 (PECAM), respectively in the thickened arterial wall. The photogram in the inset of *J* represents a normal manifestation of unaffected artery. Immunohistochemical staining with hematoxylin counter-staining. Scale bar: in *I*, 200 μm; in *J*, 100 μm.

arteries (data not shown). Degenerative or granulomatous vascular lesions were not observed in conjunction with the perivascular infiltration, indicating that the vascular lesion of interest is not related to any type of vasculitis syndrome. We found no vascular lesions in the kidney or the colon of B6.TgL mice. Thus, the spontaneous lung disease in B6.TgL mice was characterized by lung-specific, pulmonary artery-restricted intimal thickening with lymphocytic (chronic) inflammation. These histopathological characteristics are similar yet distinct in a few points from those of human PAH.

Strain-restricted onset of the lung disease

The PAH-like disease, as defined in the B6.TgL mice, was quantified with a PAH score in other strains of mice, including B6, BALB, BALB.TgL, BALB × B6.TgL (BCF1.TgL), and (BALB × B6) F1 × B6.TgL (BCN2.TgL). It was observed that wild-type and different TgL strains, such as BALB.TgL and BCF1.TgL, barely developed the PAH-like disease (Table 1). On the other hand, BCN2.TgL developed a PAH-like disease with a broader distribution of the PAH score than B6.TgL. There were no sex-related differences in the PAH scores (Table 1). These findings indicate that development of the PAH-like disease depends on both the effects of TgL and on an undefined B6-specific genetic background.

Elevation of RV systolic pressure and RV hypertrophy in B6.TgL

The PAH-like arteriopathy in B6.TgL mice indicated the onset of clinical PH. We therefore measured right ventricular (RV) systolic pressure (RVSP) in aged B6.TgL, BALB.TgL, and their wild-type strains. RVSP was significantly increased in the B6.TgL mice, as compared to B6 (Figure 2A). Importantly, the RVSP values were significantly correlated with the PAH scores (Figure 2B). Furthermore, significant RV hypertrophy was demonstrated for B6.TgL, as compared to B6 mice (Figure 2C). Increases in RVSP and RV hypertrophy were not observed in the BALB.TgL mice, as compared to B6 mice (additional file 2). In other experiments performed using wild-type BALB mice (30 w), there has been no evidence for RV hypertension or RV hypertrophy in BALB strain: RVSP = 21.3 ±2.72 mmHg, RV/(LV + IVS) = 0.25 ±0.026.

Accumulation of effector/memory $CD4^+$ T cells in OX40L-Tg mice

Previous studies performed with B6.TgL mice have demonstrated a selective increase in the number of $CD44^{high}CD62L^{low}$ effector/memory $CD4^+$ T cells in lymphoid and nonlymphoid tissues [17,19]. We examined whether the tissue distribution of effector/memory $CD4^+$ T cells was altered by the genetic background before the disease onset. Flow cytometric analyses revealed a significant increase in the number of effector/memory $CD4^+$ T cells in both the spleen (Figure 3A and 3B) and lungs (Figure 3C and 3D) in every TgL mouse examined. Importantly, this increase was not observed in a strain-specific manner, indicating that the development of PAH is not simply explained by the increase of effector/memory $CD4^+$ T cells.

Strain-specific profile of cytokine production by the lung $CD4^+$ T cells

The functionality of resident $CD4^+$ T cells in the lungs of TgL mice was determined by testing their ability to produce cytokines in response to anti-CD3 or PMA/ionomycin stimulation, respectively. Augmented IL-13 production was observed in the TgL-derived T cells and interestingly, this augmentation was greater in B6.TgL than in BALB.TgL (Figure 4A). Furthermore, a larger number of IL-17-producing $CD4^+$ T cells were observed in B6.TgL mice than in BALB.TgL (Figure 4B). IL-4 and IL-5 were not detected in stimulated lung cells by any strains (data not shown). These results indicate that the function of tissue resident CD4 T cells can be modulated by the excessive OX40 signals on B6 genetic background before disease onset.

Over-expression of OX40L in B6 background alters the balance between lung resident effector/memory T cells and regulatory T cells

$CD4^+CD25^+Foxp3^+$ T cells, usually denoted as T_{reg} cells, are known to control inflammatory responses by suppressing the activities of $Foxp3^-$ effector T cells [24]. Several independent studies have demonstrated that lung resident T_{reg} cells suppress type 2 immune responses and, consequently, reduce pulmonary inflammation [25-27]. We analyzed the population size of T_{reg} cells, defined as $CD4^+Foxp3^+$, in the lung of non-transgenic and TgL strains. Flow cytometric analyses revealed that the frequency and absolute number of T_{reg} cells increased in TgL strains in advance of the disease onset as compared with those in nontransgenic strains (Figure 5A and 5B). It was particularly noted that the increase of T_{reg} was less in B6.TgL than in BALB.TgL, suggesting that B6-specific genetic factors counteract development of T_{reg} cells in TgL mice. We also examined the ratio of Foxp3- effector/memory CD4 T cells (additional file 3) to Foxp3+ T_{reg} before disease onset. The data shows an increased ratio of effector/memory T cells to T_{reg} cells in the B6.TgL lung compared to the BALB.TgL lung (Figure 5C). These findings also suggest an important role of T_{reg} in regulating inflammation associated with the pathogenesis of PAH-like disease in B6.TgL mice.

Identification of a susceptibility locus for PAH

TgL-dependent PH developed in a strain-specific manner, suggesting that the genetic background had an effect

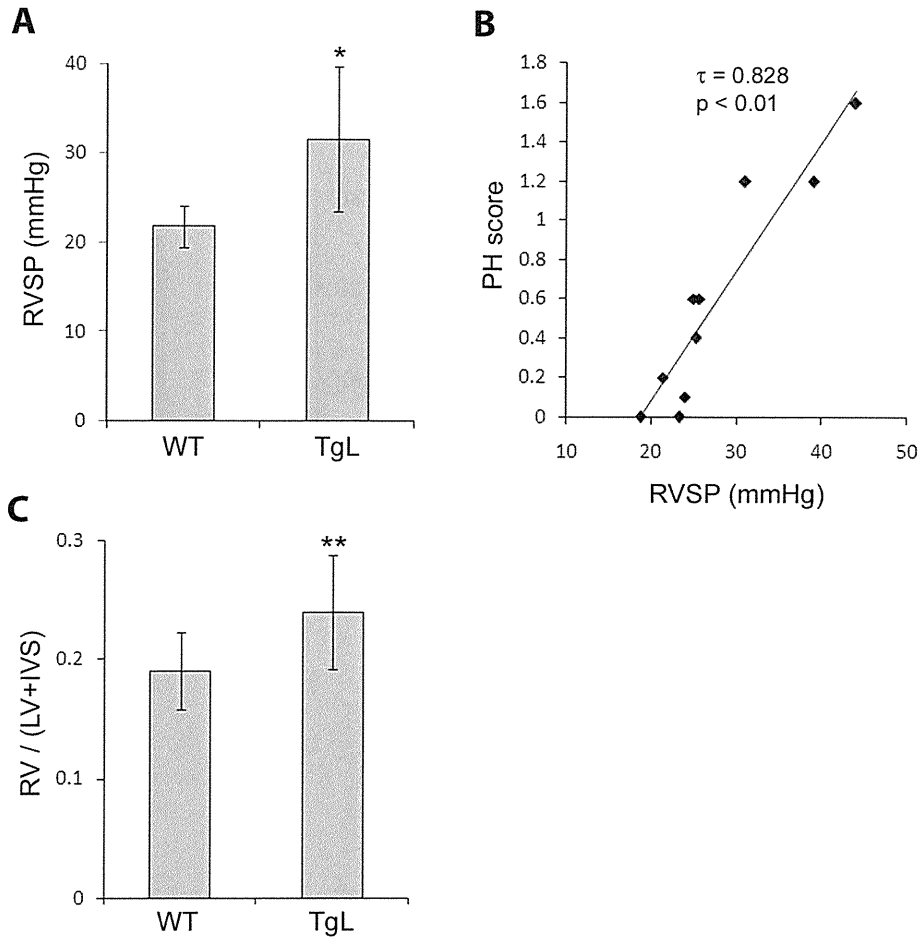

Figure 2 Clinicopathological phenotypes associated with PH. (A) Significant elevation of RVSP (mmHg) in B6.TgL. The result represents a mean ± standard deviation (SD) of 4 B6 or 6 B6.TgL mice (20 to 24 weeks old) for each group. (B) Correlation between RVSP values and PAH scores obtained from the 10 mice examined in *A*. The significance of this correlation was confirmed with the Kendall tau (τ) rank correlation coefficient (τ = 0.828). (C) RV hypertrophy manifested in B6.TgL. RV hypertrophy was evaluated with the index provided by the formula, RV/(LV+IVS). The result represents a mean ± SD of 12 B6 or 8 B6.TgL mice for each group. The significant difference between the two groups was evaluated by two-tailed *t*-test. *, $p < 0.05$; **, $p < 0.01$.

on the disease phenotypes. To identify a susceptibility locus for a PAH-like disease in B6.TgL, a genetic approach was employed using BCN2.TgL mice, which are descended from the B6.TgL and non-disease-prone BALB.TgL strains of mice. A genome-wide scan performed using selected 48 BCN2.TgL mice identified 4 candidate loci on chromosomes 5, 9, 13, and 17, which were possibly associated with the incidence of a PAH-like disease (additional file 1). The association study with 341 BCN2.TgL mice confirmed the suggestive association at *D5Mit346* (1 cM) and *D5Mit381* (8 cM) on chromosome 5 (Table 2). The other candidate loci preliminarily defined on chromosomes 9, 13, and 17 were not confirmed by this study. A QTL analysis consistently demonstrated a suggestive linkage between the level of PAH score and the chromosomal region between *D5Mit346* and *D5Mit381*. This linkage was observed in a single LOD peak of 2.4 at 7 cM on chromosome 5 (Figure 6).

Discussion

Previous studies have shown that B6.TgL mice display abnormal T-cell differentiation and functions, and spontaneous inflammation in the colon and lung. The colonic phenotype in B6.TgL mice was histopathologically defined as an inflammatory bowel disease resembling ulcerative colitis in humans. In the present study, the undetermined lung disease in B6.TgL mice was characterized as a PAH-like disease. PAH is a clinical category of PH that comprises many different disease entities. Pathological manifestations of the PAH-like disease in B6.TgL mice are not completely parallel to those of idiopathic PAH. The differences between idiopathic PAH

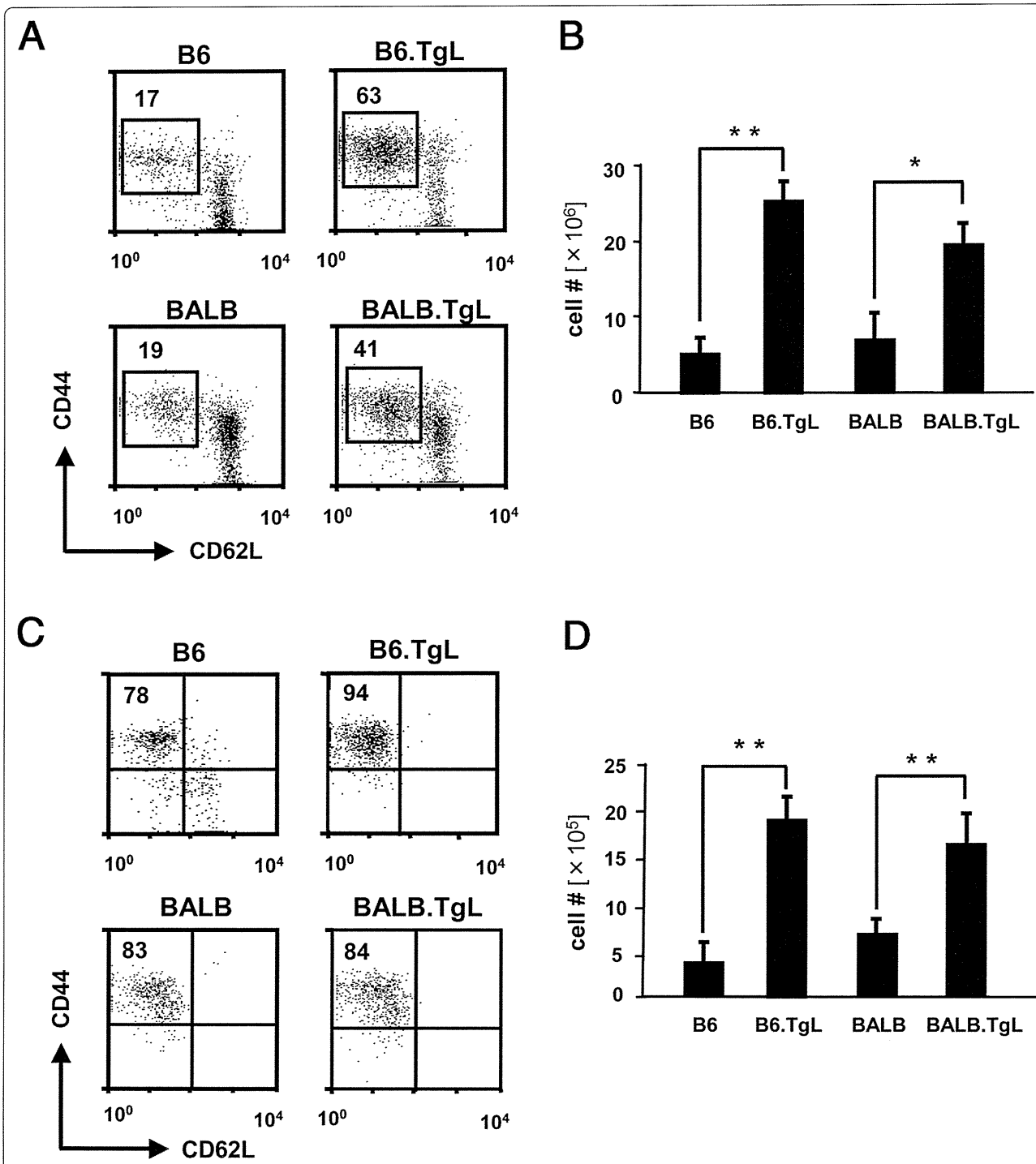

Figure 3 Accumulation of effector/memory CD4$^+$ cells in transgenic (TgL) strains of mice. The percentages of CD44^{high}CD62L^{low}CD25$^-$CD4$^+$ T cells (effector/memory CD4$^+$T cells) in a total of CD4$^+$T cells are shown in the dot grams; (A) spleen, (C) lung. The absolute numbers of effector/memory CD4$^+$ T cells are shown in the bar grams; (B) spleen, (D) lung. The absolute number was calculated from the percentage of this subset and the total cell number in each organ. The results represent a mean ± SD of 6-8 mice per each group. The results of flow cytometry (A and C) are representative of three independent experiments performed using 8 to 10 week-old mice. The significant difference between the two groups was evaluated by two tailed *t*-test. *, $p < 0.01$; **, $p < 0.001$.

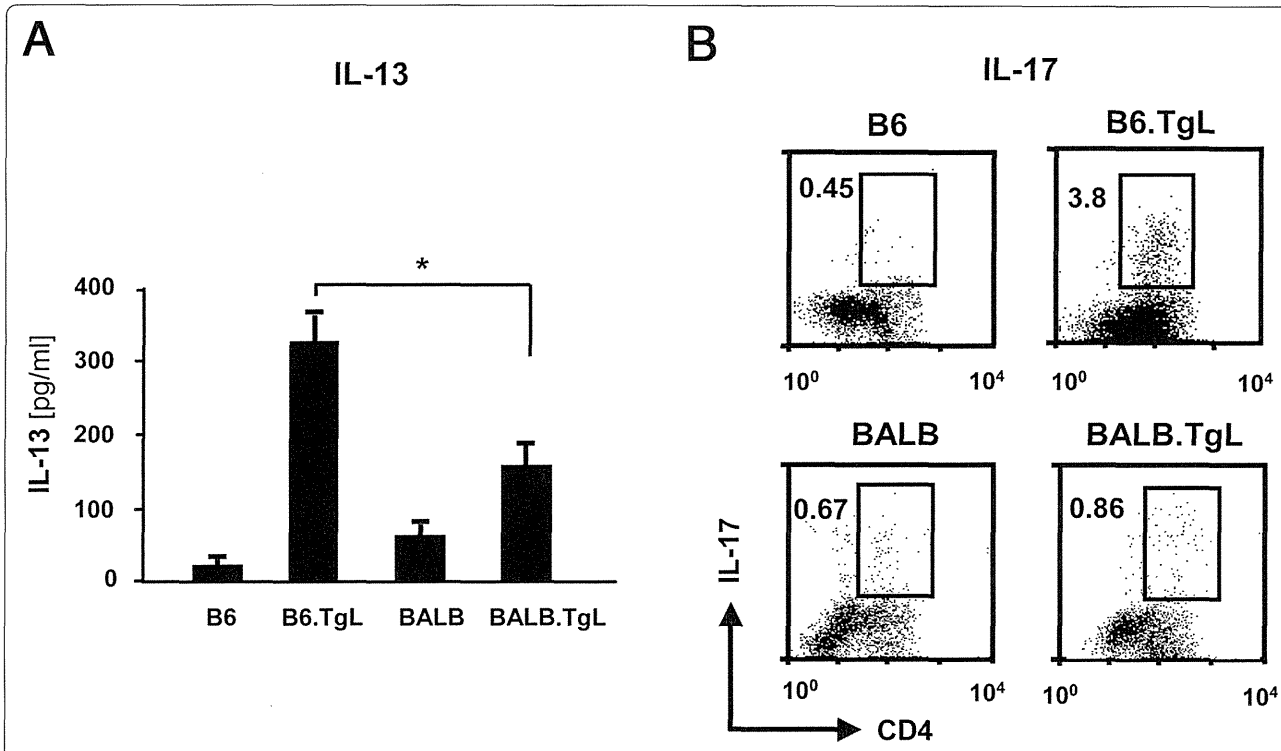

Figure 4 Strain-specific cytokine profile in lung CD4$^+$T cells. (A) IL-13 production from a total of lymphocytes isolated from the lung of non-transgenic and transgenic (TgL) strains of mice at 8 to 10 week-old. Lymphocytes containing equal number of CD44^{high}CD62L^{low}CD4$^+$T cells for each group (n = 4) of strain were stimulated with soluble anti-CD3 for 48 h and IL-13 in the cultured supernatant was quantified by ELISA. The significant difference between B6.TgL and BALB.TgL was evaluated by two-tailed *t*-test. *, $p < 0.05$. (B) IL-17 production in the lung CD4$^+$T cells. Lymphocytes isolated as above were incubated with PMA/Ionomycin in the presence of brefeldin A for 4 h and intracellular IL-17 production was analyzed in CD4 T cells. Representative data from two independent experiments were shown.

and the present animal model include the caliber of the affected arteries, the primarily affected layer of vascular wall, and the participation of massive lymphocytic perivascular infiltration. Further investigations are needed to define the present lung pathology as any type of PAH. An increasing body of evidence implicates the role of immune-mediated mechanisms in the pathogenesis of PAH. A type of PAH occurs secondarily to collagen vascular disorders, such as systemic sclerosis and mixed connective tissue disease (MCTD). Interestingly, PAH with MCTD presents with a prominent characteristic of endothelial degeneration and proliferation, probably due to the pathogenic contribution of autoantibodies to endothelial cells [28,29]. This characteristic may be a pathological consequence of immune-mediated mechanisms shared with the present model. The findings in the B6.TgL mice provide a possible insight into an implication of an OX40L-derived signal in the immune-mediated mechanism of endothelial pathology in PAH.

PAH is associated with endothelial cell dysfunction and vasoconstriction. There is no direct evidence for a link between these pulmonary vascular manifestations and abnormality *in situ* of OX40L-derived signal. However, it has been shown that OX40L-derived signals have a pathologic impact on the endothelial cell functions of systemic arteries. Recent studies have demonstrated an association of OX40L gene polymorphism with the susceptibility to atherosclerosis in humans [30], and the critical contribution of OX40-OX40L interactions to atherogenesis in low-density lipoprotein receptor-deficient mice [31]. The endothelial cells of the systemic arteries and those of the pulmonary arteries are exposed to different conditions, i.e., blood pressure and oxygen tension. It is interesting to know whether the OX40-OX40L interactions yield a different response on pulmonary endothelial cells than on systemic endothelial cells, and whether the OX40L gene polymorphism is associated with any type of PAH in humans.

Our present immunological studies performed using TgL and non-TgL strains of mice with different genetic backgrounds–B6 and BALB–revealed the respective effects of TgL and strain-dependent genetic background on immune phenotypes in the lung. Previous studies have demonstrated that OX40L-derived signals promote the expansion of effector/memory CD4$^+$ T cells [17,19]

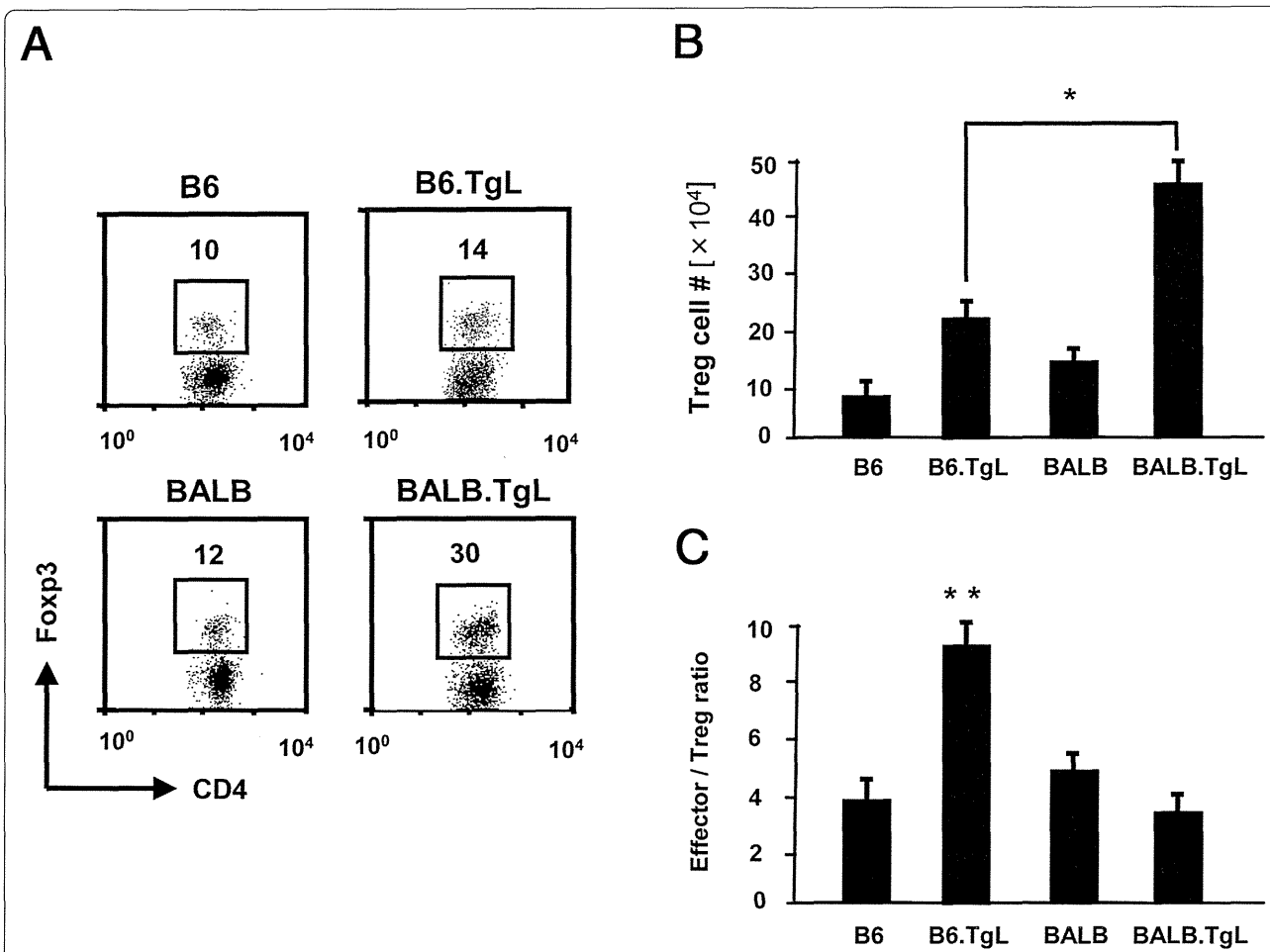

Figure 5 Accumulation of T_{reg} cells in non-transgenic and transgenic (TgL) strains of mice at 8 to 10 week-old. The percentage (A) and absolute numbers (B) of $CD4^+$ $Foxp3^+T_{reg}$ cells in the lung are shown. The absolute lymphocytic number was calculated from the percentage of T_{reg} and the total cell number. (C) The ratio of effector/memory T cells (CD4+ CD25- $CD44^{high}$ $CD62L^{low}$) to Fopx3+ T_{reg} cells in the lung. A significant increase in this ratio is shown in B6.TgL strain of mice. The result represents a mean ± SD from 4 mice per each group. The results of flow cytometry (A) are representative of two independent experiments. The significant difference between the two groups was evaluated by two tailed *t*-test. *, $p < 0.01$; **, $p < 0.001$.

and naturally arising T_{reg} cells [32], and enhance the production of IL-13 and IL-17 by $CD4^+$ T cells [33-35]. To examine which TgL-dependent immune aberrations are correlated with the onset of the PAH-like disease, we examined TgL-dependent immune phenotypes in the lungs of 2 different strains at a pre-disease stage. The findings indicate that B6-specific genetic factors influence the expansion of effector/memory $CD4^+$ T cells and T_{reg} cells in advance of the onset of lung disease. A possible role of T_{reg} cells has been documented in the

Table 2 Genetic association of PAH score in BCN2

Marker	Position (CM)	Mean of grade† BB	Mean of grade BC	P value‡
D5Mit346	1	0.51 ± 0.61 (172)	0.32 ± 0.46 (169)	0.0018 §
D5Mit381	8	0.51 ± 0.59 (178)	0.32 ± 0.46 (163)	0.0012 §
D5Mit197	36	0.46 ± 0.56 (192)	0.36 ± 0.52 (149)	0.0844
D5Mit338	59	0.45 ± 0.55 (191)	0.37 ± 0.53 (150)	0.1476
D5Mit213	70	0.41 ± 0.52 (192)	0.42 ± 0.58 (149)	0.9149
D5Mit409	83	0.42 ± 0.55 (165)	0.41 ± 0.54 (178)	0.766

* Values indicate mean ± SD and the values in parenthesis denote the number of mice.

† BB = B6 homozygote; BC = B6/BALB heterozygote

‡ The two-tail t-test. §, suggestive linkage [22].

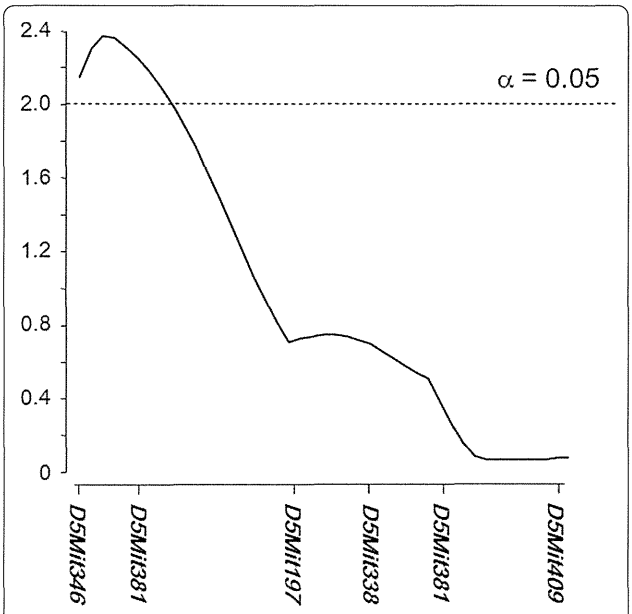

Figure 6 LOD plots of the QTL analysis for PAH scores on chromosome 5. The significant threshold level ($\alpha = 0.05$) is shown by a score of 2 with a dashed line. The LOD peak (2.4) is located at 7 cM. The Y-axis denotes the level of the LOD score, and the X-axis denotes the genetic position defined by the microsatellite markers indicated: *D5Mit346* (1 cM), *D5Mit381* (8 cM), *D5Mit197* (36 cM), *D5Mit338* (59 cM), *D5Mit213* (70 cM), and *D5Mit409* (83 cM). The results were obtained using the interval mapping program of the MapMarker/QTL software.

development of PAH in humans [6]. Furthermore, it is clearly shown that B6-specific genetic factors increase the number of IL-17-producing $CD4^+$ T cells as well as secretion of IL-13 and IFNγ (data not shown) by lung tissue resident $CD4^+$ T cells. IL-17 producing CD4 T cells, namely Th17 cells are well known that participates in the pathogenesis of various organ-specific autoimmune diseases, such as inflammatory bowel disease and rheumatoid arthritis [36,37]. Although the role of Th17 cells in PAH in humans has not been determined, our present findings suggest that they indeed play a role in PAH. IL-13 serves as an important mediator in pulmonary inflammation [5,38,39], suggesting a causal contribution of IL-13 to the pathogenesis of the present model. The presence of immunological findings provides an insight into PAH-prone immune condition in the lung: the increase of proinflammatory effectors, IL-13 and Th17, and the decrease of an anti-inflammatory effector, T_{reg}.

The present genome-wide genetic approach demonstrated a new susceptibility locus controlling the onset of a PAH-like disease in our model. Previous genetic studies performed on familial PAH have shown mutations in 2 genes responsible for susceptibility to PAH: bone morphogenetic protein receptor 2 gene (*BMPR2*) [40] and activin-like kinase type-1 gene (*ALK-1*) [41]. Our identified locus includes neither of these genes, nor, to the best of our knowledge, any gene involved in their signal transduction pathways. However, *Nos3* and *Hgf* genes were particularly noted within this locus. Nitric oxide (NO) is known as a potent endothelial cell-derived vasodilator and an inhibitor of smooth muscle proliferation. Endothelial NO production largely depends on NOS3/eNOS (encoded by *Nos3*). NOS3-deficient mice showed reduced pulmonary vascular proliferation and remodeling to chronic hypoxia [42,43]. Several studies have reported the preventive role of NO in the development of PH in mice and humans. The polymorphism of human *Nos3* gene is associated with high-altitude pulmonary edema and PH in patients with chronic obstructive pulmonary disease [44]. On the other hand, *Hgf*, which encodes hepatocyte growth factor (HGF), suppresses vascular medial hyperplasia and matrix accumulation in advanced PH in rats [45]. These findings have underscored the role of NOS3/eNOS or HGF as a pathogenic modifier in the present PH model.

A T-cell subset, type II helper T cell (Th2), plays an important role in the pathogenesis of PAH in mice [39]. In this regard, it is noteworthy that the 2 loci (the transgene locus and the susceptibility locus) have a strong impact on Th1/Th2 balance. The OX40 signal promotes a Th2-prone condition in mice [34]. On the other hand, NO and HGF serve as inducible factors for type I helper T cells (Th1) [46,47]. Therefore, in the TgL strains of mice, the 2 loci are mutually counterbalanced, and the net Th1/Th2 proportion depends mainly on the polymorphic effect of the susceptibility locus. In a B6 genetic background, an effect of the susceptibility locus may suppress Th1 responses and maximize Th2 augmentation in the lung conferred by the OX40L transgene, resulting in the B6-specific onset of PH.

Conclusion

The present study reported a novel transgenic mouse model for PH. This model differs from previous PH models, which include a hypoxia-induced model, a drug-induced model, and a genetic model (i.e., endothelin B receptor-deficient) [48], in etiology, histopathology, and spontaneity of PH. Considering the physiological functions of OX40L, it is likely that the development of PH in the present model depends on Th2-mediated mechanisms. The present model may provide a new experimental opportunity for investigating immune-mediated mechanisms underlying PAH and the development of immune-targeted therapy for PAH.

Additional material

Additional file 1: Summary of genome wide scan. Genotypes of BCN2.TgL mice were determined by polymerase chain reaction (PCR) using genomic DNA for 98 microsatellite positions.

Additional file 2: Pathological phenotypes in the lung of BALB.TgL mice. (A) RVSP (mmHg) in BALB.TgL (35 w, male, n = 4) and wild-type B6 (28 w, male, n = 4). The difference in the average values between the two strains is not statistically significant (p = 0.37, two tailed t test). These RVSP values tended to be lower than those in our previous measurement shown in Figure 2A. This change is probably due to the difference in the experimental conditions. (B) Evaluation of RV hypertrophy in BALB.TgL (35 w, male, n = 5) and wild-type B6 (28 w, male, n = 5). RV hypertrophy was evaluated with the index of RV/(LV +IVS). The difference between the two strains is not statistically significant (p = 0.76, two-tailed t-test).

Additional file 3: Foxp3 expression on total CD4 versus CD25 negative effector CD4 T cells. Total CD4 and CD4+CD62L^{low}CD25 negative cells from the lung tissue were stained for intracellular Foxp3.

List of Abbreviations

αSMA: Alpha smooth muscle actin; B6.TgL: OX40L transgenic on C75BL/6 strain; BALB. TgL: OX40L transgenic on BALB/c strain; H & E: Hematoxylin and Eosin; HGF: Hepatocyte growth factor; IVS: Intraventricular Septum; LOD: Logarithm of odd; LV: Left ventricular; MCTD: Mixed connective tissue disease; NO: Nitric oxide; OX40L: OX40 ligand; PH: Pulmonary hypertension; PAH: Pulmonary arterial hypertension; PMA: phorbol 12-myristate 13-acetate; QTL: quantitative trait locus; RV: Right ventricle; RVSP: Right ventricular systolic pressure; Th: T helper cells; T reg: regulatory T cell; TNFSF: Tumor necrosis super-family

Acknowledgements

We would like to thank Drs. Mingcai Zhang, Hiroshi Furukawa, Hiroyuki Kumagai, Shigeki Shibahara, Yasushi Hoshikawa, and Masahisa Kyogoku for providing helpful, critical comments, Mr. Shin-ichi Tanaka and Miss Naomi Yamaki for technical help in the RVSP measurement, and Mrs. Emi Yura for secretarial help. This work was supported by grants: No.19390108 & No.19659096, Grants-in-Aid for Scientific Research from the Ministry of Education, Science, Sports, and Culture of Japan. CREST, JST.

Author details

[1]Department of Pathology, Tohoku University Graduate School of Medicine, 2-1 Seiryo, Aoba-ku, Sendai, Miyagi 980-8575 Japan. [2]Department of Immunology, Tohoku University Graduate School of Medicine, 2-1 Seiryo, Aoba-ku, Sendai, Miyagi 980-8575 Japan. [3]Department of Cardiovascular Medicine, Tohoku University Graduate School of Medicine, 2-1 Seiryo, Aoba-ku, Sendai, Miyagi 980-8575 Japan. [4]Department of Pharmacology and Medicine and Center for Lung Biology, University of South Alabama, College of Medicine, 307 University Blvd N Mobile, AL 36688-0002 USA. [5]Department of Pathology, Ehime University Graduate School of Medicine, Shitsukawa, Toon, Ehime 791-0295 Japan. [6]Japan Science and Technology Agency, CREST, Tokyo, Japan. [7]Johnson & Johnson Pharmaceutical Research & Development, L.L.C., 3210 Merryfield Row, San Diego, California 92121, USA.

Authors' contributions

MR and MO (Ono) conceived the project and contributed to all the aspect of this research. MN contributed to the genetic findings. MY, MO (Oka), and IFM contributed to histopathological findings. PS, NI, and KS (Sugamura) contributed to immunological findings. KS (Satoh) and HS contributed to physical findings such as blood pressure measurements. All authors read and approved the final manuscript.

Competing interests

The authors declare that they have no competing interests.

Received: 16 June 2011 Accepted: 15 December 2011
Published: 15 December 2011

References

1. Veeraraghavan S, Koss MN, Sharma OP: **Pulmonary veno-occlusive disease.** *Curr Opin Pulm Med* 1999, **5(5)**:310-313.
2. Dorfmuller P, Perros F, Balabanian K, Humbert M: **Inflammation in pulmonary arterial hypertension.** *Eur Respir J* 2003, **22(2)**:358-363.
3. Humbert M, Morrell NW, Archer SL, Stenmark KR, MacLean MR, Lang IM, Christman BW, Weir EK, Eickelberg O, Voelkel NF, *et al*: **Cellular and molecular pathobiology of pulmonary arterial hypertension.** *J Am Coll Cardiol* 2004, **43(12 Suppl S)**:13S-24S.
4. Golembeski SM, West J, Tada Y, Fagan KA: **Interleukin-6 causes mild pulmonary hypertension and augments hypoxia-induced pulmonary hypertension in mice.** *Chest* 2005, **128(6 Suppl)**:572S-573S.
5. Hoshino T, Kato S, Oka N, Imaoka H, Kinoshita T, Takei S, Kitasato Y, Kawayama T, Imaizumi T, Yamada K, *et al*: **Pulmonary Inflammation and Emphysema: Role of the Cytokines IL-18 and IL-13.** *Am J Respir Crit Care Med* 2007, **176(1)**:49-62.
6. Nicolls MR, Taraseviciene-Stewart L, Rai PR, Badesch DB, Voelkel NF: **Autoimmunity and pulmonary hypertension: a perspective.** *Eur Respir J* 2005, **26(6)**:1110-1118.
7. Taraseviciene-Stewart L, Nicolls MR, Kraskauskas D, Scerbavicius R, Burns N, Cool C, Wood K, Parr JE, Boackle SA, Voelkel NF: **Absence of T cells confers increased pulmonary arterial hypertension and vascular remodeling.** *Am J Respir Crit Care Med* 2007, **175(12)**:1280-1289.
8. Lenschow DJ, Walunas TL, Bluestone JA: **CD28/B7 system of T cell costimulation.** *Annu Rev Immunol* 1996, **14**:233-258.
9. Croft M: **Co-stimulatory members of the TNFR family: keys to effective T-cell immunity?** *Nat Rev Immunol* 2003, **3(8)**:609-620.
10. Sugamura K, Ishii N, Weinberg AD: **Therapeutic targeting of the effector T-cell co-stimulatory molecule OX40.** *Nat Rev Immunol* 2004, **4(6)**:420-431.
11. Mestas J, Crampton SP, Hori T, Hughes CC: **Endothelial cell co-stimulation through OX40 augments and prolongs T cell cytokine synthesis by stabilization of cytokine mRNA.** *Int Immunol* 2005, **17(6)**:737-747.
12. Kotani A, Hori T, Matsumura Y, Uchiyama T: **Signaling of gp34 (OX40 ligand) induces vascular endothelial cells to produce a CC chemokine RANTES/CCL5.** *Immunol Lett* 2002, **84(1)**:1-7.
13. Gramaglia I, Weinberg AD, Lemon M, Croft M: **Ox-40 ligand: a potent costimulatory molecule for sustaining primary CD4 T cell responses.** *J Immunol* 1998, **161(12)**:6510-6517.
14. Murata K, Ishii N, Takano H, Miura S, Ndhlovu LC, Nose M, Noda T, Sugamura K: **Impairment of antigen-presenting cell function in mice lacking expression of OX40 ligand.** *J Exp Med* 2000, **191(2)**:365-374.
15. Rogers PR, Song J, Gramaglia I, Killeen N, Croft M: **OX40 promotes Bcl-xL and Bcl-2 expression and is essential for long-term survival of CD4 T cells.** *Immunity* 2001, **15(3)**:445-455.
16. Soroosh P, Ine S, Sugamura K, Ishii N: **OX40-OX40 ligand interaction through T cell-T cell contact contributes to CD4 T cell longevity.** *J Immunol* 2006, **176(10)**:5975-5987.
17. Soroosh P, Ine S, Sugamura K, Ishii N: **Differential Requirements for OX40 Signals on Generation of Effector and Central Memory CD4+ T Cells.** *J Immunol* 2007, **179(8)**:5014-5023.
18. Maxwell JR, Weinberg A, Prell RA, Vella AT: **Danger and OX40 receptor signaling synergize to enhance memory T cell survival by inhibiting peripheral deletion.** *J Immunol* 2000, **164(1)**:107-112.
19. Murata K, Nose M, Ndhlovu LC, Sato T, Sugamura K, Ishii N: **Constitutive OX40/OX40 ligand interaction induces autoimmune-like diseases.** *J Immunol* 2002, **169(8)**:4628-4636.
20. Satoh K, Kagaya Y, Nakano M, Ito Y, Ohta J, Tada H, Karibe A, Minegishi N, Suzuki N, Yamamoto M, *et al*: **Important role of endogenous erythropoietin system in recruitment of endothelial progenitor cells in hypoxia-induced pulmonary hypertension in mice.** *Circulation* 2006, **113(11)**:1442-1450.
21. Marzo AL, Vezys V, Williams K, Tough DF, Lefrancois L: **Tissue-level regulation of Th1 and Th2 primary and memory CD4 T cells in response to Listeria infection.** *J Immunol* 2002, **168(9)**:4504-4510.
22. Lander E, Kruglyak L: **Genetic dissection of complex traits: guidelines for interpreting and reporting linkage results.** *Nat Genet* 1995, **11(3)**:241-247.
23. Morris JA, Gardner MJ: **Calculating confidence intervals for relative risks (odds ratios) and standardised ratios and rates.** *Br Med J (Clin Res Ed)* 1988, **296(6632)**:1313-1316.
24. Sakaguchi S: **Naturally arising CD4+ regulatory t cells for immunologic self-tolerance and negative control of immune responses.** *Annu Rev Immunol* 2004, **22**:531-562.
25. Hadeiba H, Locksley RM: **Lung CD25 CD4 regulatory T cells suppress type 2 immune responses but not bronchial hyperreactivity.** *J Immunol* 2003, **170(11)**:5502-5510.

26. Lewkowich IP, Herman NS, Schleifer KW, Dance MP, Chen BL, Dienger KM, Sproles AA, Shah JS, Kohl J, Belkaid Y, *et al*: **CD4+CD25+ T cells protect against experimentally induced asthma and alter pulmonary dendritic cell phenotype and function.** *J Exp Med* 2005, **202(11)**:1549-1561.
27. McKinley L, Logar AJ, McAllister F, Zheng M, Steele C, Kolls JK: **Regulatory T cells dampen pulmonary inflammation and lung injury in an animal model of pneumocystis pneumonia.** *J Immunol* 2006, **177(9)**:6215-6226.
28. Bodolay E, Csipo I, Gal I, Sipka S, Gyimesi E, Szekanecz Z, Szegedi G: **Anti-endothelial cell antibodies in mixed connective tissue disease: frequency and association with clinical symptoms.** *Clin Exp Rheumatol* 2004, **22(4)**:409-415.
29. Vegh J, Szodoray P, Kappelmayer J, Csipo I, Udvardy M, Lakos G, Aleksza M, Soltesz P, Szilagyi A, Zeher M, *et al*: **Clinical and immunoserological characteristics of mixed connective tissue disease associated with pulmonary arterial hypertension.** *Scand J Immunol* 2006, **64(1)**:69-76.
30. Wang X, Ria M, Kelmenson PM, Eriksson P, Higgins DC, Samnegard A, Petros C, Rollins J, Bennet AM, Wiman B, *et al*: **Positional identification of TNFSF4, encoding OX40 ligand, as a gene that influences atherosclerosis susceptibility.** *Nat Genet* 2005, **37(4)**:365-372.
31. van Wanrooij EJ, van Puijvelde GH, de Vos P, Yagita H, van Berkel TJ, Kuiper J: **Interruption of the Tnfrsf4/Tnfsf4 (OX40/OX40L) pathway attenuates atherogenesis in low-density lipoprotein receptor-deficient mice.** *Arterioscler Thromb Vasc Biol* 2007, **27(1)**:204-210.
32. Takeda I, Ine S, Killeen N, Ndhlovu LC, Murata K, Satomi S, Sugamura K, Ishii N: **Distinct roles for the OX40-OX40 ligand interaction in regulatory and nonregulatory T cells.** *J Immunol* 2004, **172(6)**:3580-3589.
33. Ohshima Y, Yang LP, Uchiyama T, Tanaka Y, Baum P, Sergerie M, Hermann P, Delespesse G: **OX40 costimulation enhances interleukin-4 (IL-4) expression at priming and promotes the differentiation of naive human CD4(+) T cells into high IL-4-producing effectors.** *Blood* 1998, **92(9)**:3338-3345.
34. Hoshino A, Tanaka Y, Akiba H, Asakura Y, Mita Y, Sakurai T, Takaoka A, Nakaike S, Ishii N, Sugamura K, *et al*: **Critical role for OX40 ligand in the development of pathogenic Th2 cells in a murine model of asthma.** *Eur J Immunol* 2003, **33(4)**:861-869.
35. Nakae S, Saijo S, Horai R, Sudo K, Mori S, Iwakura Y: **IL-17 production from activated T cells is required for the spontaneous development of destructive arthritis in mice deficient in IL-1 receptor antagonist.** *Proc Natl Acad Sci USA* 2003, **100(10)**:5986-5990.
36. Kotake S, Udagawa N, Takahashi N, Matsuzaki K, Itoh K, Ishiyama S, Saito S, Inoue K, Kamatani N, Gillespie MT, *et al*: **IL-17 in synovial fluids from patients with rheumatoid arthritis is a potent stimulator of osteoclastogenesis.** *J Clin Invest* 1999, **103(9)**:1345-1352.
37. Fujino S, Andoh A, Bamba S, Ogawa A, Hata K, Araki Y, Bamba T, Fujiyama Y: **Increased expression of interleukin 17 in inflammatory bowel disease.** *Gut* 2003, **52(1)**:65-70.
38. Zhu Z, Ma B, Zheng T, Homer RJ, Lee CG, Charo IF, Noble P, Elias JA: **IL-13-induced chemokine responses in the lung: role of CCR2 in the pathogenesis of IL-13-induced inflammation and remodeling.** *J Immunol* 2002, **168(6)**:2953-2962.
39. Daley E, Emson C, Guignabert C, de Waal Malefyt R, Louten J, Kurup VP, Hogaboam C, Taraseviciene-Stewart L, Voelkel NF, Rabinovitch M, *et al*: **Pulmonary arterial remodeling induced by a Th2 immune response.** *J Exp Med* 2008, **205(2)**:361-372.
40. Deng Z, Morse JH, Slager SL, Cuervo N, Moore KJ, Venetos G, Kalachikov S, Cayanis E, Fischer SG, Barst RJ, *et al*: **Familial primary pulmonary hypertension (gene PPH1) is caused by mutations in the bone morphogenetic protein receptor-II gene.** *Am J Hum Genet* 2000, **67(3)**:737-744.
41. Morse JH, Deng Z, Knowles JA: **Genetic aspects of pulmonary arterial hypertension.** *Ann Med* 2001, **33(9)**:596-603.
42. Quinlan TR, Li D, Laubach VE, Shesely EG, Zhou N, Johns RA: **eNOS-deficient mice show reduced pulmonary vascular proliferation and remodeling to chronic hypoxia.** *Am J Physiol Lung Cell Mol Physiol* 2000, **279(4)**:L641-650.
43. Steudel W, Scherrer-Crosbie M, Bloch KD, Weimann J, Huang PL, Jones RC, Picard MH, Zapol WM: **Sustained pulmonary hypertension and right ventricular hypertrophy after chronic hypoxia in mice with congenital deficiency of nitric oxide synthase 3.** *J Clin Invest* 1998, **101(11)**:2468-2477.
44. Droma Y, Hanaoka M, Ota M, Katsuyama Y, Koizumi T, Fujimoto K, Kobayashi T, Kubo K: **Positive association of the endothelial nitric oxide synthase gene polymorphisms with high-altitude pulmonary edema.** *Circulation* 2002, **106(7)**:826-830.
45. Ono M, Sawa Y, Mizuno S, Fukushima N, Ichikawa H, Bessho K, Nakamura T, Matsuda H: **Hepatocyte growth factor suppresses vascular medial hyperplasia and matrix accumulation in advanced pulmonary hypertension of rats.** *Circulation* 2004, **110(18)**:2896-2902.
46. Ito W, Kanehiro A, Matsumoto K, Hirano A, Ono K, Maruyama H, Kataoka M, Nakamura T, Gelfand EW, Tanimoto M: **Hepatocyte growth factor attenuates airway hyperresponsiveness, inflammation, and remodeling.** *Am J Respir Cell Mol Biol* 2005, **32(4)**:268-280.
47. Niedbala W, Wei XQ, Campbell C, Thomson D, Komai-Koma M, Liew FY: **Nitric oxide preferentially induces type 1 T cell differentiation by selectively up-regulating IL-12 receptor beta 2 expression via cGMP.** *Proc Natl Acad Sci USA* 2002, **99(25)**:16186-16191.
48. Ivy DD, McMurtry IF, Colvin K, Imamura M, Oka M, Lee DS, Gebb S, Jones PL: **Development of occlusive neointimal lesions in distal pulmonary arteries of endothelin B receptor-deficient rats: a new model of severe pulmonary arterial hypertension.** *Circulation* 2005, **111(22)**:2988-2996.

doi:10.1186/1471-2172-12-67
Cite this article as: Rabieyousefi *et al.*: Indispensable roles of OX40L-derived signal and epistatic genetic effect in immune-mediated pathogenesis of spontaneous pulmonary hypertension. *BMC Immunology* 2011 **12**:67.

blood

2010 116: 1971-1979
Prepublished online June 10, 2010;
doi:10.1182/blood-2010-02-269134

PKCζ decreases eNOS protein stability via inhibitory phosphorylation of ERK5

Patrizia Nigro, Jun-ichi Abe, Chang-Hoon Woo, Kimio Satoh, Carolyn McClain, Michael R. O'Dell, Hakjoo Lee, Jae-Hyang Lim, Jian-dong Li, Kyung-Sun Heo, Keigi Fujiwara and Bradford C. Berk

Blood (print ISSN 0006-4971, online ISSN 1528-0020), is published weekly by the American Society of Hematology, 2021 L St, NW, Suite 900, Washington DC 20036.

specific expression of protein kinase Akt. *J Clin Invest*. 2006;116:334–343.
22. Korshunov VA, Berk BC. Flow-induced vascular remodeling in the mouse: a model for carotid intima-media thickening. *Arterioscler Thromb Vasc Biol*. 2003;23:2185–2191.
23. Ishida M, Ishida T, Thomas S, Berk BC. Activation of extracellular signal-regulated kinases (ERK1/2) by angiotensin II is dependent on c-Src in vascular smooth muscle cells. *Circ Res*. 1998;82:7–12.
24. Ishida T, Ishida M, Suero J, Takahashi M, Berk BC. Agonist-stimulated cytoskeletal reorganization and signal transduction at focal adhesions in vascular smooth muscle cells require c-Src. *J Clin Invest*. 1999;103:789–797.
25. Jin ZG, Berk BC. SOXF: redox mediators of vascular smooth muscle cell growth. *Heart*. 2004;90:488–490.
26. Tolbert T, Thompson J, Bouchard P, Oparil S. Estrogen-induced vasoprotection is independent of inducible nitric oxide synthase expression: evidence from the mouse carotid artery ligation model. *Circulation*. 2001;104:2740–2745.
27. Payeli SK, Schiene-Fischer C, Steffel J, Camici GG, Rozenberg I, Luscher TF, Tanner FC. Cyclophilin A differentially activates monocytes and endothelial cells: role of purity, activity, and endotoxin contamination in commercial preparations. *Atherosclerosis*. 2008;197:564–571.
28. Schafer K, Schroeter MR, Dellas C, Puls M, Nitsche M, Weiss E, Hasenfuss G, Konstantinides SV. Plasminogen activator inhibitor-1 from bone marrow-derived cells suppresses neointimal formation after vascular injury in mice. *Arterioscler Thromb Vasc Biol*. 2006;26:1254–1259.
29. Wang CH, Anderson N, Li SH, Szmitko PE, Cherng WJ, Fedak PW, Fazel S, Li RK, Yau TM, Weisel RD, Stanford WL, Verma S. Stem cell factor deficiency is vasculoprotective: unraveling a new therapeutic potential of imatinib mesylate. *Circ Res*. 2006;99:617–625.
30. Hansson GK, Libby P. The immune response in atherosclerosis: a double-edged sword. *Nat Rev Immunol*. 2006;6:508–519.
31. Tanaka K, Sata M, Hirata Y, Nagai R. Diverse contribution of bone marrow cells to neointimal hyperplasia after mechanical vascular injuries. *Circ Res*. 2003;93:783–790.
32. Billich A, Winkler G, Aschauer H, Rot A, Peichl P. Presence of cyclophilin A in synovial fluids of patients with rheumatoid arthritis. *J Exp Med*. 1997;185:975–980.

CLINICAL PERSPECTIVE

Decreased blood flow distal to a stenosis is associated with accelerated atherosclerosis and occlusion, but the mechanisms are not fully elucidated. Accumulating evidence indicates that inflammation and vascular smooth muscle cell (VSMC) proliferation contributes to vessel narrowing. It has become clear that an increase in reactive oxygen species is a key pathogenic mechanism for vascular disease. Cyclophilin A (CyPA) is a 20-kDa chaperone protein secreted from VSMCs in response to reactive oxygen species that stimulates VSMC proliferation and inflammatory cell migration in vitro. Here, using genetically engineered mice to modulate vascular CyPA expression, we show that decreasing CyPA has beneficial effects on the inflammatory response and vascular intima formation in low-flow vessels, as shown by significantly increased lumen diameter and decreased intima/media ratio. The present study may have important clinical implications, because it appears that secreted CyPA mediates the growth and inflammation observed in low-flow vessels. This suggests that a receptor for CyPA may represent an attractive therapeutic target for vascular diseases associated with oxidative stress and inflammation.

and decreased chemotactic signaling in the absence of CyPA. Because decreased myelopoiesis could also explain diminished inflammatory cell recruitment in CyPA$^{-/-}$ mice, we analyzed white blood cell counts from mice with WT or CyPA$^{-/-}$ bone marrow. The number of circulating monocytes was not altered by CyPA deficiency or by carotid ligation. Thus, lack of CyPA in bone marrow cells does not alter inflammatory cell production or ability to enter the peripheral circulation. In contrast to the situation in CyPA$^{-/-}$ mice, VSMC-specific overexpression of CyPA (VSMC-Tg) further enhanced the accumulation of inflammatory cells in ligated carotids, which supports the important role for CyPA in mediating the recruitment of inflammatory cells.

CyPA is expressed by all cell types that participate in vascular pathology.[25] Additionally, extracellular CyPA has recently been found to induce interleukin-6 release in inflammatory cells.[27] We observed significant accumulation of inflammatory cells in the intima. We propose that ROS generated locally by inflammatory cells causes VSMCs to release CyPA, which would promote a proinflammatory cycle for vascular remodeling. Therefore, in addition to VSMC-derived CyPA, the contribution of inflammatory cells is important for intima formation in this model. Recent observations support the contribution of inflammatory cells to intimal thickening.[28,29] CyPA could regulate the proteolytic activity necessary for the migration of inflammatory cells through activating MMPs, especially MMP-1 and MMP-9.[14,16] Considering the importance of migrating inflammatory cells in vascular remodeling,[30,31] local cytokine production by inflammatory cells could promote intima formation in this model.

Study Limitations

CyPA is a chaperone protein that is widely expressed, including inflammatory cells and ECs. Therefore, CyPA in macrophages and ECs may play an important role in vascular remodeling. Future studies will be required to define the role of CyPA in the response to vascular injury of cells such as macrophages, T and B cells, mast cells, platelets, and vascular progenitor cells.

Clinical Implications and Conclusions

The present data from the use of genetically engineered mice to modulate vascular CyPA expression prove that a decrease in CyPA levels has beneficial effects on the inflammatory response and vascular intima formation, as shown by significantly increased lumen diameter and decreased I/M ratio. This is consistent with our findings that the plasma level of CyPA is increased in patients with acute coronary syndromes.[13] Additionally, Billich et al[32] reported increased concentrations of CyPA in synovial fluids of patients with rheumatoid arthritis. These results suggest that extracellular CyPA is a novel mediator for vascular disease associated with ROS and inflammation.

Acknowledgments

We are grateful to the Aab Cardiovascular Research Institute members for useful suggestions and Chris Ashley, Robert Winterkorn, Mary A. Georger, Tamlyn Thomas, and Sarah A. Mack for technical assistance.

Sources of Funding

This work was supported by National Institutes of Health grant HL49192 (to Dr Berk) and a Japan Heart Foundation/Bayer Yakuhin research grant abroad (to Dr Satoh).

Disclosures

None.

References

1. Shimokawa H. Primary endothelial dysfunction: atherosclerosis. *J Mol Cell Cardiol*. 1999;31:23–37.
2. Clempus RE, Griendling KK. Reactive oxygen species signaling in vascular smooth muscle cells. *Cardiovasc Res*. 2006;71:216–225.
3. Griendling KK, FitzGerald GA. Oxidative stress and cardiovascular injury: part I: basic mechanisms and in vivo monitoring of ROS. *Circulation*. 2003;108:1912–1916.
4. Leopold JA, Loscalzo J. Oxidative enzymopathies and vascular disease. *Arterioscler Thromb Vasc Biol*. 2005;25:1332–1340.
5. Baas AS, Berk BC. Differential activation of mitogen-activated protein kinases by H_2O_2 and O_2- in vascular smooth muscle cells. *Circ Res*. 1995;77:29–36.
6. Rao GN, Berk BC. Active oxygen species stimulate vascular smooth muscle cell growth and proto-oncogene expression. *Circ Res*. 1992;70:593–599.
7. Ross R. Atherosclerosis: an inflammatory disease. *N Engl J Med*. 1999;340:115–126.
8. Festa A, D'Agostino R, Howard G, Mykkanen L, Tracy RP, Haffner SM. Inflammation and microalbuminuria in nondiabetic and type 2 diabetic subjects: the Insulin Resistance Atherosclerosis Study. *Kidney Int*. 2000;58:1703–1710.
9. Libby P, Ridker PM. Novel inflammatory markers of coronary risk: theory versus practice. *Circulation*. 1999;100:1148–1150.
10. Jin ZG, Melaragno MG, Liao DF, Yan C, Haendeler J, Suh YA, Lambeth JD, Berk BC. Cyclophilin A is a secreted growth factor induced by oxidative stress. *Circ Res*. 2000;87:789–796.
11. Liao D-F, Jin Z-G, Baas AS, Daum G, Gygi SP, Aebersold R, Berk BC. Purification and identification of secreted oxidative stress-induced factors from vascular smooth muscle cells. *J Biol Chem*. 2000;275:189–196.
12. Suzuki J, Jin Z-G, Meoli DF, Matoba T, Berk BC. Cyclophilin A is secreted by a vesicular pathway in vascular smooth muscle cells. *Circ Res*. 2006;98:811–817.
13. Jin ZG, Lungu AO, Xie L, Wang M, Wong C, Berk BC. Cyclophilin A is a proinflammatory cytokine that activates endothelial cells. *Arterioscler Thromb Vasc Biol*. 2004;24:1186–1191.
14. Kim H, Kim WJ, Jeon ST, Koh EM, Cha HS, Ahn KS, Lee WH. Cyclophilin A may contribute to the inflammatory processes in rheumatoid arthritis through induction of matrix degrading enzymes and inflammatory cytokines from macrophages. *Clin Immunol*. 2005;116:217–224.
15. Damsker JM, Bukrinsky MI, Constant SL. Preferential chemotaxis of activated human CD4$^+$ T cells by extracellular cyclophilin A. *J Leukoc Biol*. 2007;82:613–618.
16. Zhu P, Ding J, Zhou J, Dong WJ, Fan CM, Chen ZN. Expression of CD147 on monocytes/macrophages in rheumatoid arthritis: its potential role in monocyte accumulation and matrix metalloproteinase production. *Arthritis Res Ther*. 2005;7:R1023–R1033.
17. Novak A, Guo C, Yang W, Nagy A, Lobe CG. Z/EG, a double reporter mouse line that expresses enhanced green fluorescent protein upon Cre-mediated excision. *Genesis*. 2000;28:147–155.
18. Sakai K, Mitani K, Miyazaki J. Efficient regulation of gene expression by adenovirus vector-mediated delivery of the CRE recombinase. *Biochem Biophys Res Commun*. 1995;217:393–401.
19. Miano JM, Ramanan N, Georger MA, de Mesy Bentley KL, Emerson RL, Balza RO Jr, Xiao Q, Weiler H, Ginty DD, Misra RP. Restricted inactivation of serum response factor to the cardiovascular system. *Proc Natl Acad Sci U S A*. 2004;101:17132–17137.
20. Kumar A, Hoover JL, Simmons CA, Lindner V, Shebuski RJ. Remodeling and neointimal formation in the carotid artery of normal and P-selectin–deficient mice. *Circulation*. 1997;96:4333–4342.
21. Mukai Y, Rikitake Y, Shiojima I, Wolfrum S, Satoh M, Takeshita K, Hiroi Y, Salomone S, Kim HH, Benjamin LE, Walsh K, Liao JK. Decreased vascular lesion formation in mice with inducible endothelial-

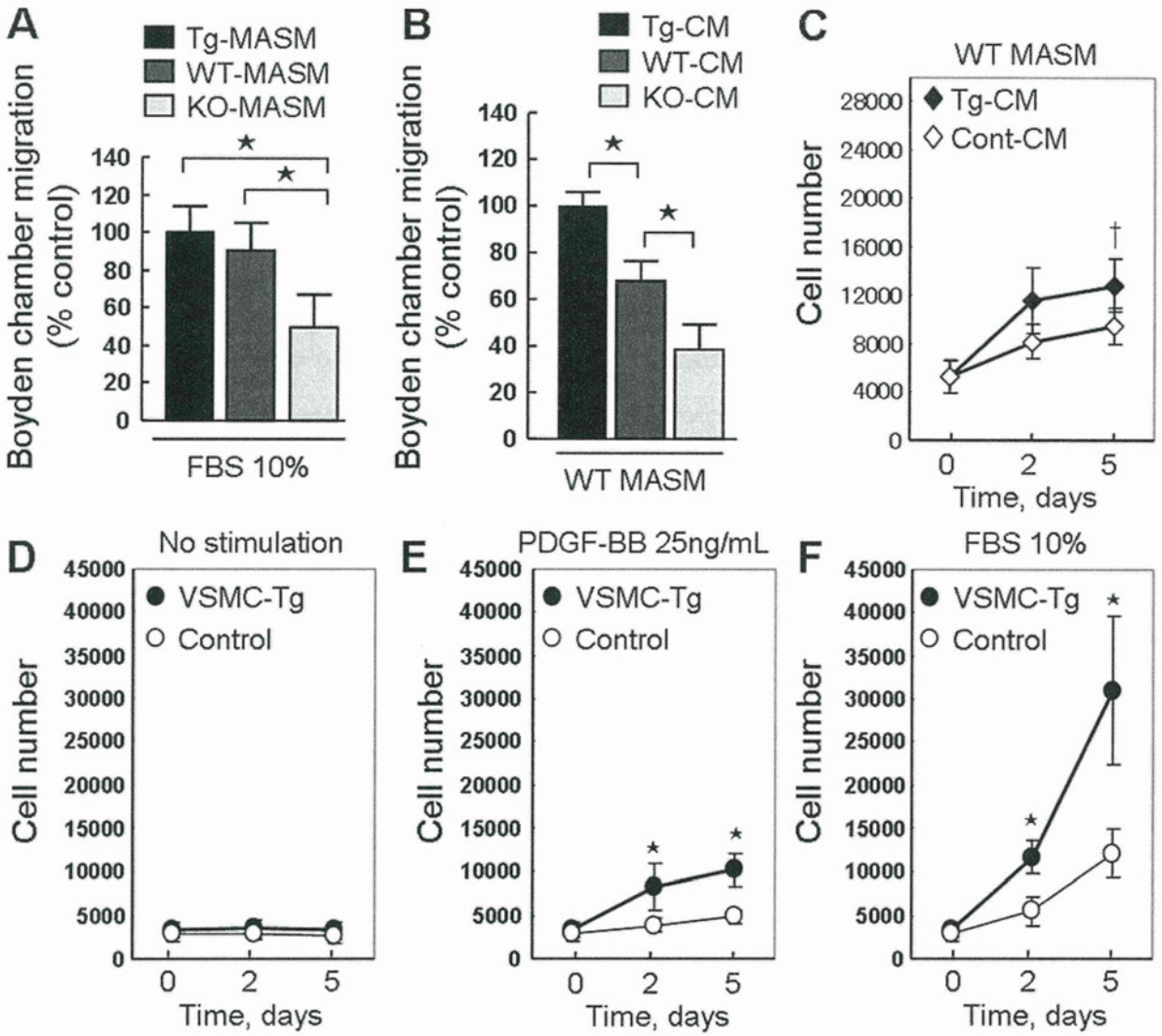

Figure 8. CyPA promotes migration and proliferation of MASMs. A, Migration of MASMs in response to 10% fetal bovine serum (FBS) in Boyden chamber assay. Tg-MASMs, WT-MASMs, and KO-MASMs were starved overnight and then seeded in the upper Boyden chamber on collagen-precoated PVP-free polycarbonate membranes. FBS (10%) was added to the lower chamber. Migration was determined, and the maximum increase was normalized to 100%. B, WT-MASMs were starved overnight and then seeded in the upper Boyden chamber. Tg-CM, WT-CM, or KO-CM was added to the lower chamber. Cells were incubated for 8 hours at 37°C in a 95% air/5% CO_2 humidified incubator. The membranes were removed, and cells were stained. The relative increases in cell number were determined by quantitative densitometry. *$P<0.01$. Data are mean±SD; n=6 in each group. C, CM from VSMC-Tg (Tg-CM) or control (Cont-CM) promotes cell proliferation. WT-MASMs were seeded in 96-well plates in DMEM supplemented with 10% FBS, serum starved for 24 hours, and stimulated with Tg-CM or Cont-CM for 5 days. CM was changed at day 3, and cells were counted at day 2 and day 5. Data are mean±SD. †$P<0.05$. D–F, Effect of platelet-derived growth factor-BB (PDGF-BB) and FBS on proliferation of Tg-MASMs and control MASMs. After starvation for 24 hours, MASMs were incubated with DMEM (D) or stimulated with 25 ng/mL PDGF-BB (E) or 10% FBS (F) for 5 days. Medium was changed at day 3, and cells were counted at day 2 and day 5. Data are mean±SD. *$P<0.01$. n=8 in each group.

by Ki67 correlated significantly with CyPA expression (VSMC-Tg>control WT>CyPA$^{-/-}$). VSMC migration and chemotaxis similarly correlated with the magnitude of CyPA expression. The increased VSMC proliferation and migration that resulted from VSMC-specific overexpression of CyPA suggests a major contribution for VSMC-derived CyPA in vascular remodeling.

Turbulent blood flow and reduced shear stress generate ROS and play a crucial role in the development of atherosclerosis due to local inflammation.[7–9] In VSMCs, ROS activate a pathway that induces secretion of CyPA,[12] which stimulates at least 3 signaling pathways (ERK1/2, Akt, and JAK).[10] Extracellular CyPA activates proinflammatory pathways in ECs, including increased expression of VCAM-1.[13] Additionally, CyPA itself is a chemoattractant and promotes migration of several cell types in vitro.[13–15] Consistently, carotid ligation increased VCAM-1 expression in ligated WT carotids. VCAM-1 expression was significantly less in ligated CyPA$^{-/-}$ carotids, which corresponded to reduced accumulation of CD45^{+} cells in the intima. This implies that the decreased accumulation of inflammatory cells in CyPA$^{-/-}$ carotids likely results from reduced expression of VCAM-1

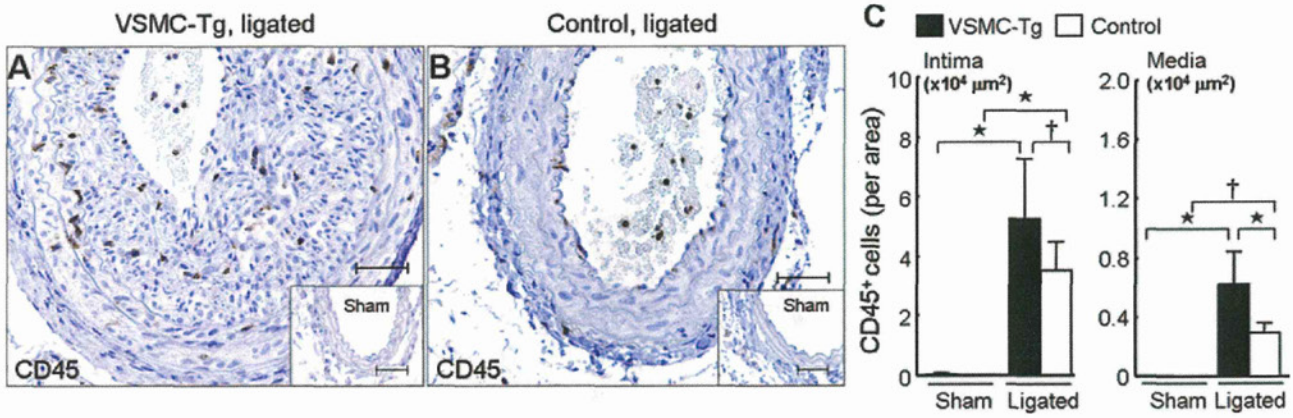

Figure 6. Overexpression of CyPA promotes recruitment of inflammatory cells in ligated carotids. Representative immunostaining of CD45 in ligated arteries from VSMC-Tg (A) and control mice (B). C, Number of CD45$^+$ cells in VSMC-Tg (n=7, solid bars) and control mice (n=6, open bars). VSMC-specific overexpression of CyPA enhanced the recruitment of CD45$^+$ cells to the intima and media. Results are mean±SD. *P<0.01; †P<0.05.

carotids, whereas ligated carotids showed increases of 217% in intimal area, 32% in medial area, and 140% in I/M ratio compared with control mice expressing normal levels of CyPA. The observation that VSMC-specific CyPA overexpression increased not only the medial area but also the intimal area suggests that VSMC-derived extracellular CyPA promotes the proliferation and migration of VSMCs via a secreted, paracrine pathway. VSMC proliferation measured

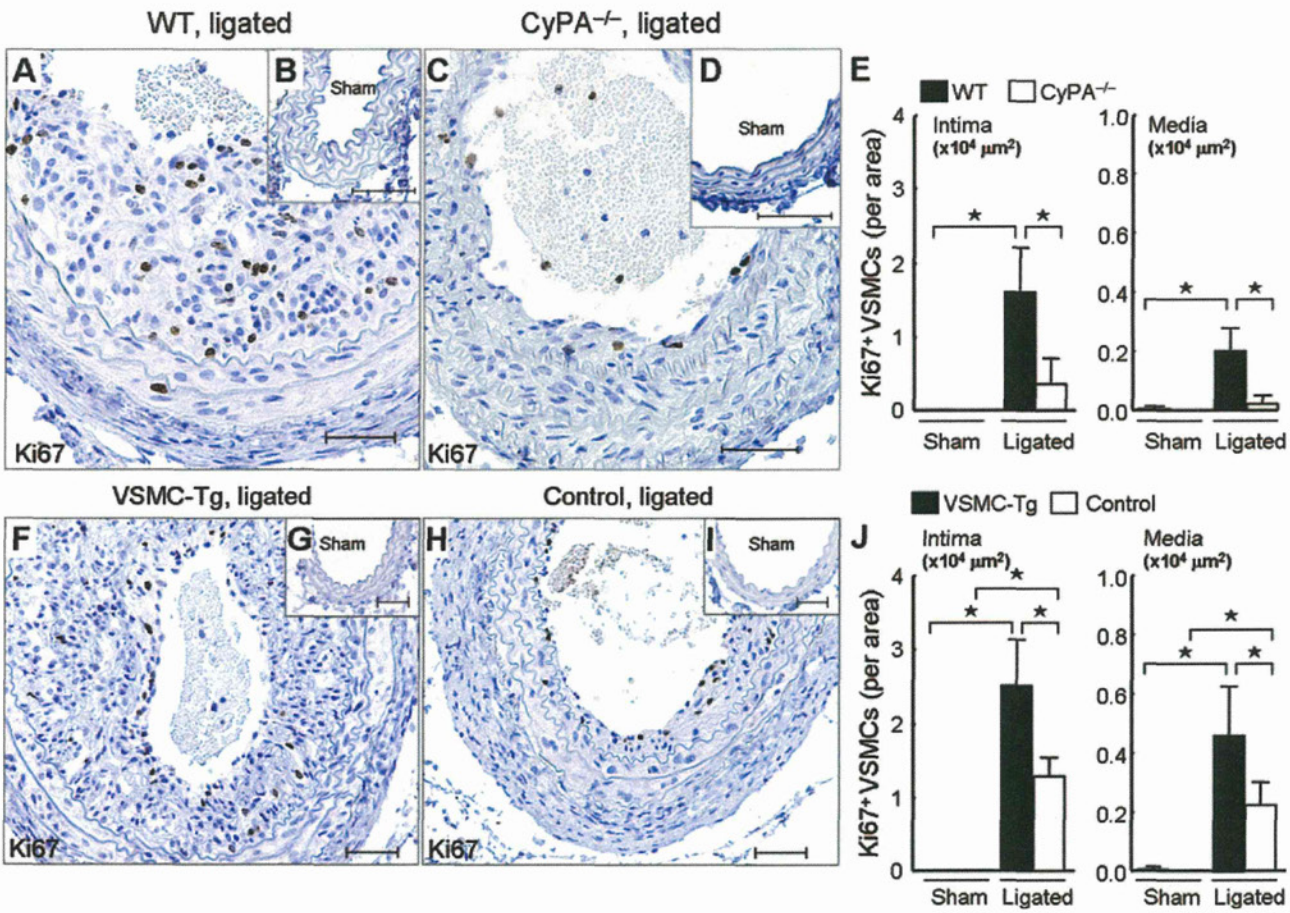

Figure 7. CyPA increases VSMC proliferation in ligated carotids. Representative immunostaining of Ki67 and counterstaining with hematoxylin in sham carotids and ligated carotids from WT, CyPA$^{-/-}$, VSMC-Tg, and control mice. A–E, There were a significantly increased number of Ki67$^+$ cells in ligated WT carotids (n=9, solid bars) compared with CyPA$^{-/-}$ carotids (n=8, open bars). Scale bars=50 μm. E, Analysis of numbers of α-SMA$^+$ Ki67$^+$ cells by staining of serial section (3 sections per mouse) was performed. F–J, There was a significant increase in Ki67$^+$ VSMCs in ligated VSMC-Tg carotids (n=7, solid bars) compared with control carotids (n=6, open bars). J, Analysis of numbers of α-SMA$^+$ Ki67$^+$ cells by staining of serial section (3 sections per mouse) was performed. Results are mean±SD. *P<0.01.

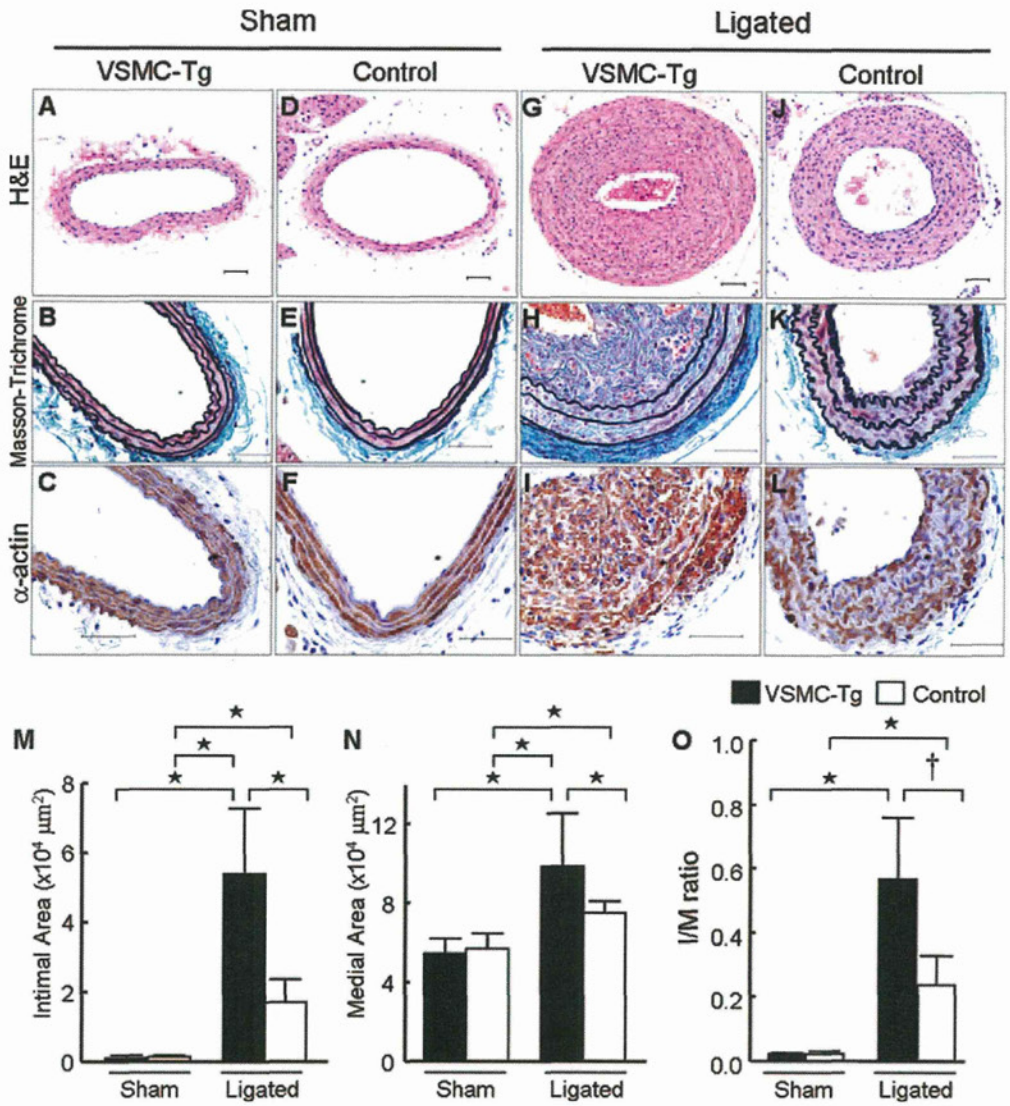

Figure 5. VSMC-specific overexpressed CyPA increases vascular remodeling after carotid ligation. Photomicrographs from sham (A–F) and ligated (G–L) mice carotids of VSMC-Tg and control. The predominant cellular component in the intima was VSMC, as revealed by immunostaining for α-SMA (α-actin). H&E indicates hematoxylin and eosin staining. Scale bars=50 μm. Intima (M), media (N), and adventitia area (O) in VSMC-Tg mice (n=7, solid bars) were greater than in control mice (n=6, open bars). Results are mean±SD. *$P<0.01$; †$P<0.05$.

Discussion

The major findings of the present study are that carotid ligation increases CyPA expression in the vascular wall and promotes vascular remodeling due to proliferation and migration of VSMCs and accumulation of inflammatory cells. These results are the first direct demonstration that CyPA contributes to vascular remodeling in vivo. The present study revealed 3 important pathological consequences of CyPA activity (Data Supplement Figure VI). First, VSMC-derived secreted CyPA increases intimal VSMCs by virtue of its ability to promote VSMC proliferation and migration. Second, secreted extracellular CyPA is proinflammatory, because it stimulates vascular expression of VCAM-1 and recruits inflammatory cells. Third, we showed a direct role for intracellular ROS to stimulate CyPA secretion that was proportionate to intracellular CyPA expression. These data show a role for CyPA as one of the key mediators of the pathological effects of ROS on vascular remodeling.

To strengthen the link between flow cessation, CyPA expression, and cell growth, we observed the time course and distribution of CyPA expression in carotids after ligation. There was minimal staining of CyPA in sham carotids but a dramatic increase in the intima and media after ligation. In parallel with CyPA expression, carotid ligation induced phosphorylation of ERK1/2 in WT carotids, which was significantly less in $CyPA^{-/-}$ carotids, consistent with the reduced number of $Ki67^+$ VSMCs in ligated $CyPA^{-/-}$ carotids. The distribution of $Ki67^+$ cells closely overlapped with areas of highest CyPA expression, especially in the rapidly proliferating intimal cells in WT mice (Data Supplement Figure III). Colocalization of CyPA and α-SMA staining revealed that CyPA expression was particularly high in VSMCs (Data Supplement Figure III). To further prove the contribution of VSMC-derived CyPA to vascular remodeling, we prepared VSMC-specific CyPA transgenic mice (VSMC-Tg). VSMC-Tg mice exhibited no significant change in sham

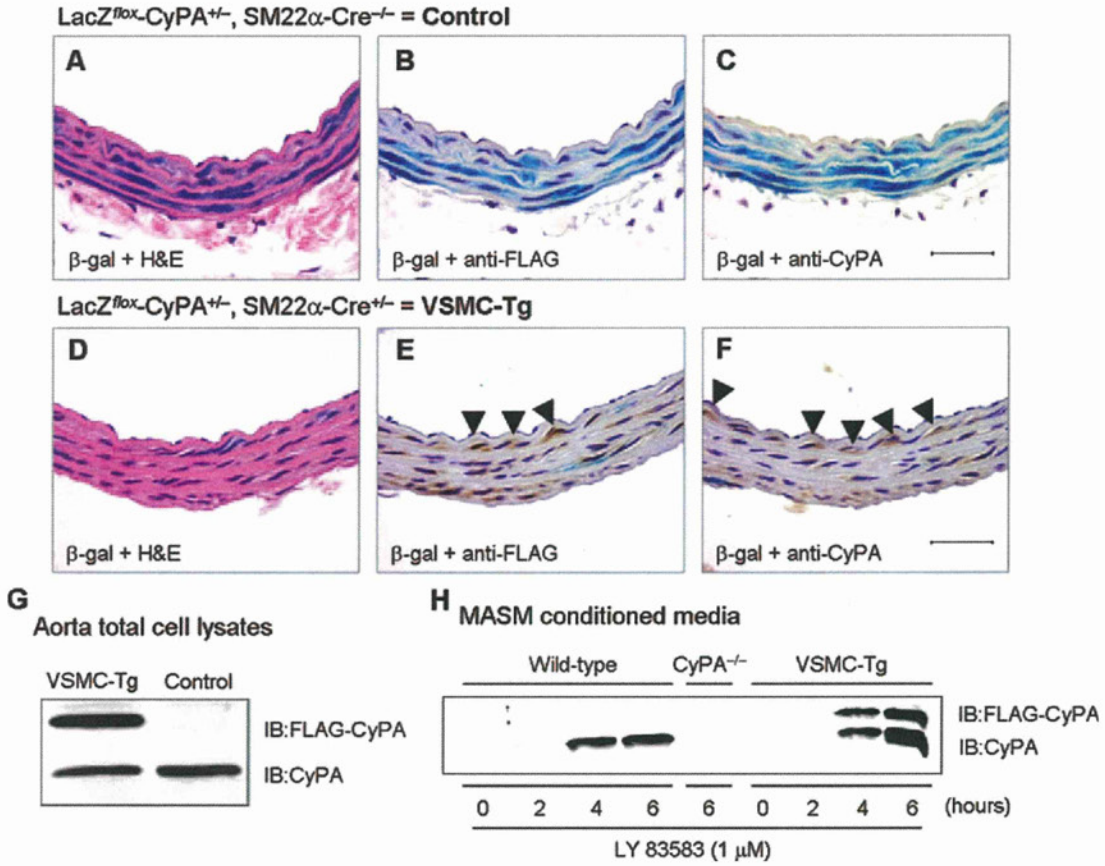

Figure 4. Characterization of CyPA expression in VSMC-Tg mice. A–F, Representative immunostaining and β-gal staining of aorta from VSMC-Tg mice (LacZ^{flox}-CyPA^{+}/SM22α-Cre^{+}) and control mice (LacZ^{flox}-CyPA^{+}/SM22α-Cre^{-}). β-Gal staining shows >90% expression only in VSMCs (B) and complete excision with SM22α-Cre (E). FLAG-CyPA was expressed only in VSMC-Tg mice and not in control mice. There was no change in endogenous CyPA expression. Scale bars=50 μm. G, Western blot demonstrated that FLAG-CyPA was expressed only in VSMC-Tg mice aorta, not in control mice. H, MASMs were stimulated with 1 μmol/L LY83583 for the indicated times, CM were prepared, and secreted CyPA and FLAG-CyPA were detected by Western blotting. IB indicates immunoblot; H&E, hematoxylin and eosin.

Ki67^{+} VSMCs were significantly increased in ligated WT carotids compared with CyPA$^{-/-}$ carotids (Figure 7A, 7C, and 7E). VSMC proliferation was even further enhanced in VSMC-Tg carotids compared with control carotids (Figure 7F through 7J), which suggests that CyPA promotes VSMC proliferation in vivo.

CyPA Plays a Crucial Role in Migration, Chemotaxis, and Proliferation of VSMCs In Vitro

To further confirm the role of CyPA in VSMC proliferation and migration, we harvested MASMs from the 3 mice strains and evaluated their proliferation and migration. To evaluate the effect of CyPA on VSMC migration and chemotaxis, we performed scratch-wound and Boyden chamber assays. The scratch wound was performed with WT-MASM as the "responder" cells and CM from the 3 strains. Tg-CM stimulated migration more than control-CM, and WT-CM stimulated migration more than KO-CM, which suggests that CyPA secreted into CM increased VSMC migration (Data Supplement Figure V). To measure the effect of CyPA on VSMC chemotaxis, we studied migration in response to serum and CM (Figure 8A and 8B). As anticipated, chemotaxis of KO-MASM was significantly reduced compared with WT-MASM and Tg-MASM in response to 10% serum, which suggests a role for intracellular CyPA in chemotaxis (Figure 8A). Next, we compared the chemotactic activity of CM from the 3 strains using WT-MASM as reporter cells. Migration of WT-MASM in response to Tg-CM was significantly increased compared with WT-CM (Figure 8B) and was dramatically greater than migration induced by KO-CM. These results indicate that secreted CyPA strongly enhances VSMC chemotaxis.

To determine the effect of varying CyPA secretion on VSMC growth, we measured the effects of CM on cell growth. Proliferation of WT-MASM in response to CM from Tg-MASM was significantly greater than that in response to CM from control-MASM (Figure 8C), which suggests that extracellular CyPA promotes VSMC growth. To assess the effect of CyPA expression on cell growth, we studied the ability of MASM from different strains to respond to both platelet-derived growth factor and serum (Figure 8D, 8E, and 8F). In the absence of exogenous growth stimuli, there was no difference in growth of cells isolated from VSMC-Tg compared with control (Figure 8D); however, growth in response to platelet-derived growth factor-BB and 10% serum was significantly increased in VSMC-Tg compared with control (Figure 8E and 8F). These data suggest that the level of CyPA expression has powerful effects on VSMC proliferation.

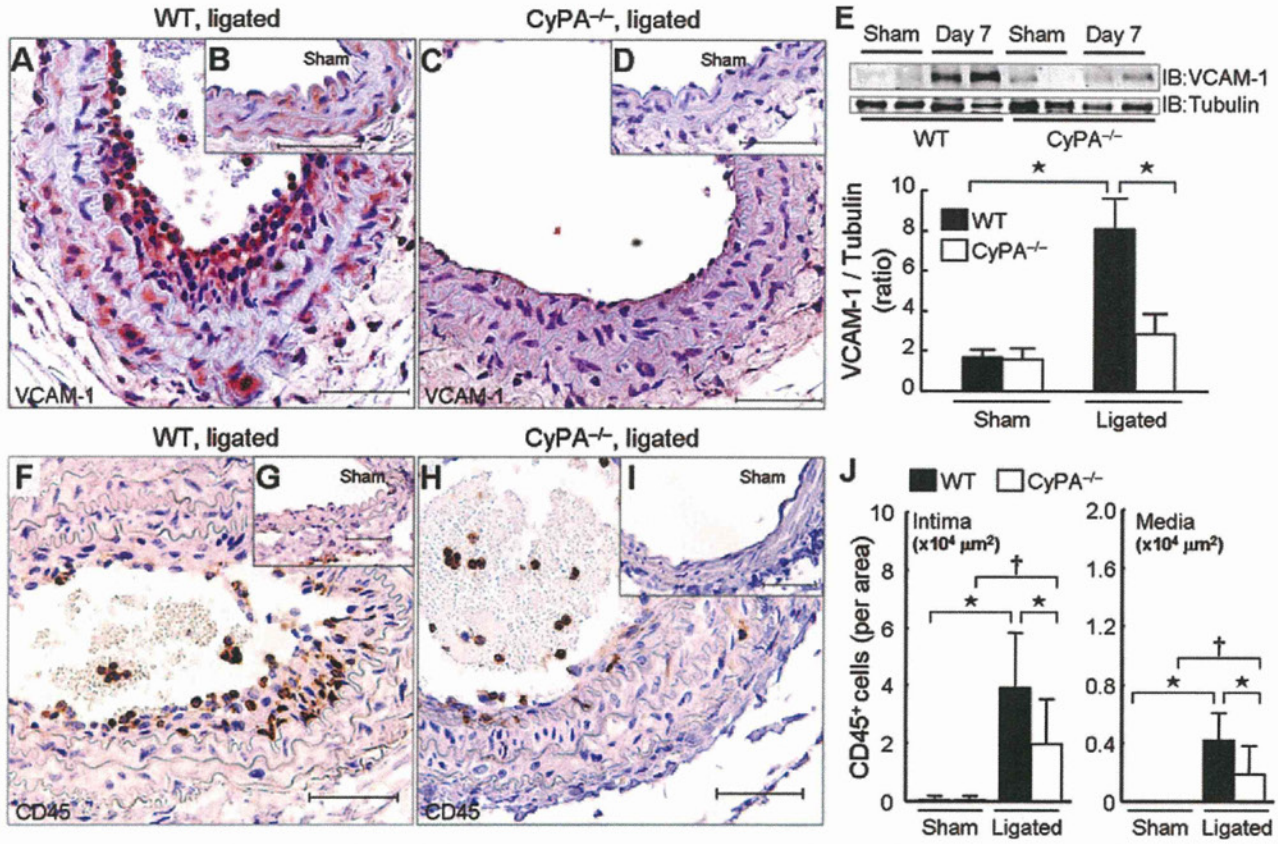

Figure 3. CyPA expression correlated with VCAM-1 expression and inflammatory cell accumulation. Representative immunostaining of VCAM-1 (A–D) and CD45 (F–I) in sham and ligated carotids from WT and CyPA$^{-/-}$ mice. Scale bars=50 μm. E, Western blot comparison of VCAM-1 in carotid homogenates of WT (n=8, solid bars) and CyPA$^{-/-}$ mice (n=6, open bars) at 7 days after ligation. Equal protein loading was confirmed with tubulin. J, The number of CD45$^+$ cells in intima and media is increased by ligation in WT mice (n=9, solid bars) and was significantly less in CyPA$^{-/-}$ mice (n=8, open bars). Results are mean±SD. *P<0.01; †P<0.05. IB indicates immunoblot.

LacZ), and the expression of exogenous FLAG-CyPA was 2-fold greater than that of endogenous CyPA. To show that FLAG-CyPA was secreted similarly to endogenous CyPA, we stimulated VSMCs harvested from aorta of WT, CyPA$^{-/-}$, and VSMC-Tg mice with LY83583. LY83583 is a naphthoquinolinedione that undergoes futile redox cycling–generating intracellular ROS.[10,11] As expected, both FLAG-CyPA and endogenous CyPA were secreted in response to ROS in MASMs from VSMC-Tg aorta (Figure 4H). The magnitude of secreted FLAG-CyPA was equivalent to that of endogenous CyPA, similar to the expression of CyPA in lysates of intact aorta (Figure 4G).

VSMC-Specific CyPA Transgenic Mice Exhibit Dramatic Intimal and Medial Thickening

To prove further that VSMC-derived CyPA promotes vascular remodeling, we performed complete carotid ligation in VSMC-Tg (LacZ^{flox}-CyPA$^+$/SM22α-Cre$^+$) and control (LacZ^{flox}-CyPA$^+$/SM22α-Cre$^-$) mice. In sham arteries, intimal thickening was not observed in VSMC-Tg and control mice (Figure 5A through 5F), and the medial area did not differ significantly (Figure 5M and 5N). Two weeks after carotid ligation, intimal thickness was significantly increased in VSMC-Tg mice to a much greater extent than in control mice (Figure 5G through 5M). Additionally, we observed significantly increased medial thickening in VSMC-Tg mice (Figure 5N). The increased intima formation was due to VSMCs, as revealed by immunostaining for α-SMA (Figure 5H and 5I). The I/M ratio was increased 2.5-fold in VSMC-Tg, which suggests a pathogenic role for VSMC-derived CyPA in accumulation of VSMCs during vascular remodeling (Figure 5O). Inflammatory cell accumulation in the remodeled carotid wall was also increased significantly in VSMC-Tg mice (Figure 6), which suggests that VSMC-derived CyPA recruits inflammatory cells.

CyPA Plays a Crucial Role in VSMC Proliferation In Vivo

To strengthen the link between CyPA expression and VSMC growth, we carefully evaluated proliferation of VSMC by immunostaining for α-SMA, Ki67, and ERK1/2 phosphorylation (pERK1/2) on serial sections. We previously reported that ERK1/2 phosphorylation is important for VSMC migration and growth.[23] There was no difference in pERK1/2 expression (Data Supplement Figure IV, B and D) or Ki67$^+$ VSMCs in sham carotids (Figure 7B and 7D); however, immunostaining and Western blotting revealed that pERK1/2 increased after carotid ligation in WT mice, with the highest expression in the intima compared with CyPA$^{-/-}$ carotids (Data Supplement Figure IV, A, C, E, and F). Consistently,

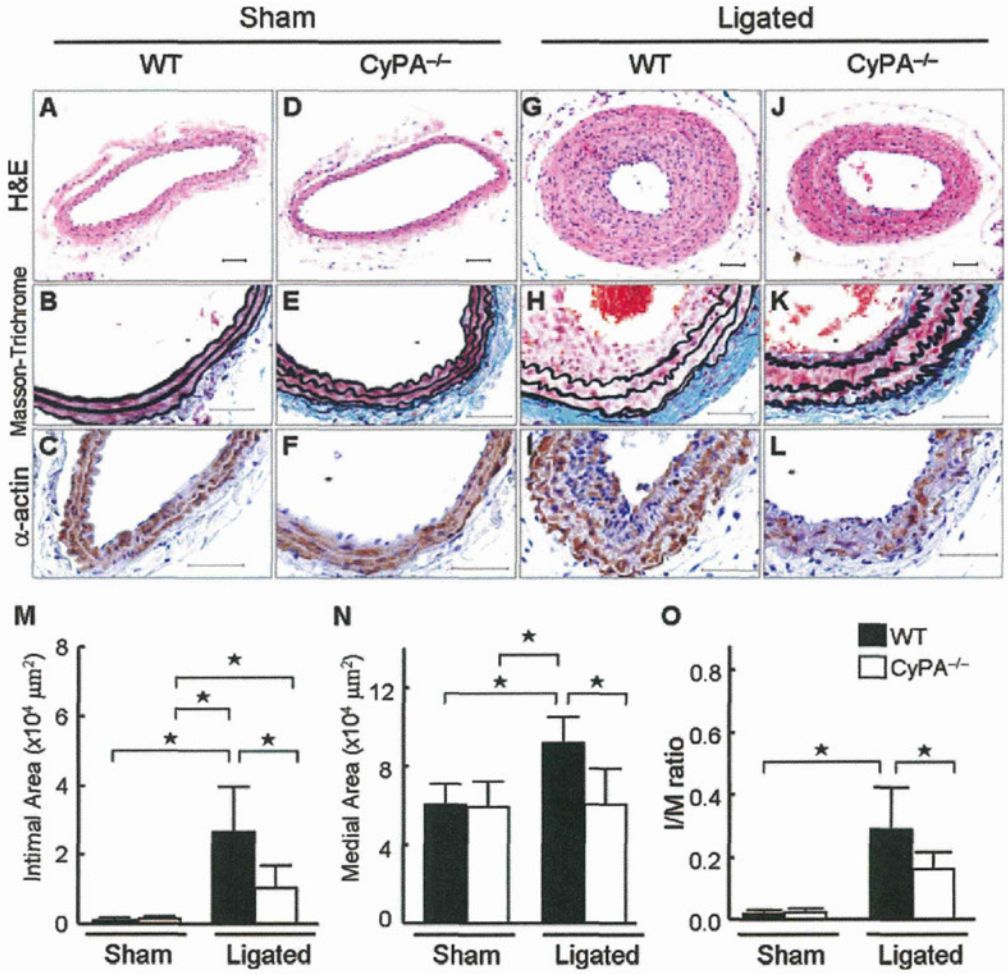

Figure 2. CyPA expression correlates with vascular remodeling. A–F, Photomicrographs showing representative cross-sectional areas of sham carotids of WT and CyPA$^{-/-}$ mice. The predominant cellular component in the intima was VSMC, as revealed by immunostaining for α-SMA. Scale bars=50 μm. G–L, Photomicrographs showing representative cross-sectional areas of ligated carotids of WT and CyPA$^{-/-}$ mice. CyPA deficiency significantly reduced intimal area (M), medial area (N), and I/M ratio (O) in CyPA$^{-/-}$ mice (n=8, open bars) compared with WT mice (n=9, solid bars). Results are mean±SD. *P<0.01. H&E indicates hematoxylin and eosin.

vein ECs[13] and is chemotactic for inflammatory cells,[14,15] we anticipated differences in inflammation based on CyPA expression. Expression of VCAM-1 was greatly increased in ligated WT carotids compared with sham (Figure 3A, 3B, and 3E). There was no difference in VCAM-1 expression in the sham carotids of WT versus CyPA$^{-/-}$ mice (Figure 3E). In contrast, expression of VCAM-1 was much lower in ligated carotids of CyPA$^{-/-}$ mice than in WT mice (Figure 3C, 3D, and 3E). The number of CD45^{+} inflammatory cells did not differ in sham arteries from WT versus CyPA$^{-/-}$ mice (Figure 3G and 3I). There was a significant increase in CD45^{+} cells in ligated arteries of WT mice (Figure 3F and 3G), whereas there was only a small change in CyPA$^{-/-}$ mice (Figure 3H and 3I). Quantification of CD45^{+} cells per intimal or medial area showed a 2-fold greater number in WT than in CyPA$^{-/-}$ mice (Figure 3J). These data suggest a role for CyPA in expression of VCAM-1 and inflammatory cell migration after carotid ligation.

Generation of VSMC-Specific CyPA Transgenic Mice

To test the hypothesis that VSMC-derived CyPA plays a major role in vascular remodeling, we prepared VSMC-Tg mice that overexpressed a FLAG-tagged CyPA only in VSMCs using a Cre/LoxP system. In brief, a LacZ^{flox}-CyPA construct (Data Supplement Figure I) was prepared with the pZ/EG vector, and LacZ^{flox}-CyPA mice were crossed with SM22α-Cre mice to achieve VSMC-specific expression. The vessels in Figure 4A through 4C are from control mice (LacZ^{flox}-CyPA^{+}/SM22α-Cre^{-}) in which the transgene expressed is LacZ, as shown by the blue β-gal staining and the low level of CyPA expression. Figure 4E shows the efficiency of Cre recombinase–mediated excision in vivo after mice were bred with SM22α-Cre to express FLAG-CyPA (SM22α-Cre×LacZ^{flox}-CyPA). Specifically, there was no LacZ expressed, as shown by β-gal staining, whereas anti-FLAG revealed significant FLAG-CyPA expression. The increase in CyPA was confirmed by anti-CyPA antibody (Figure 4F). To quantify FLAG-CyPA expression, we performed Western blots with anti-FLAG and anti-CyPA antibody. As shown in Figure 4G, the relative expression of exogenous CyPA (FLAG tagged) was 2.0-fold greater (in aorta) than that of endogenous CyPA. These experiments show that excision by SM22α-Cre was highly efficient (>90% of cells expressed FLAG, and <10% expressed

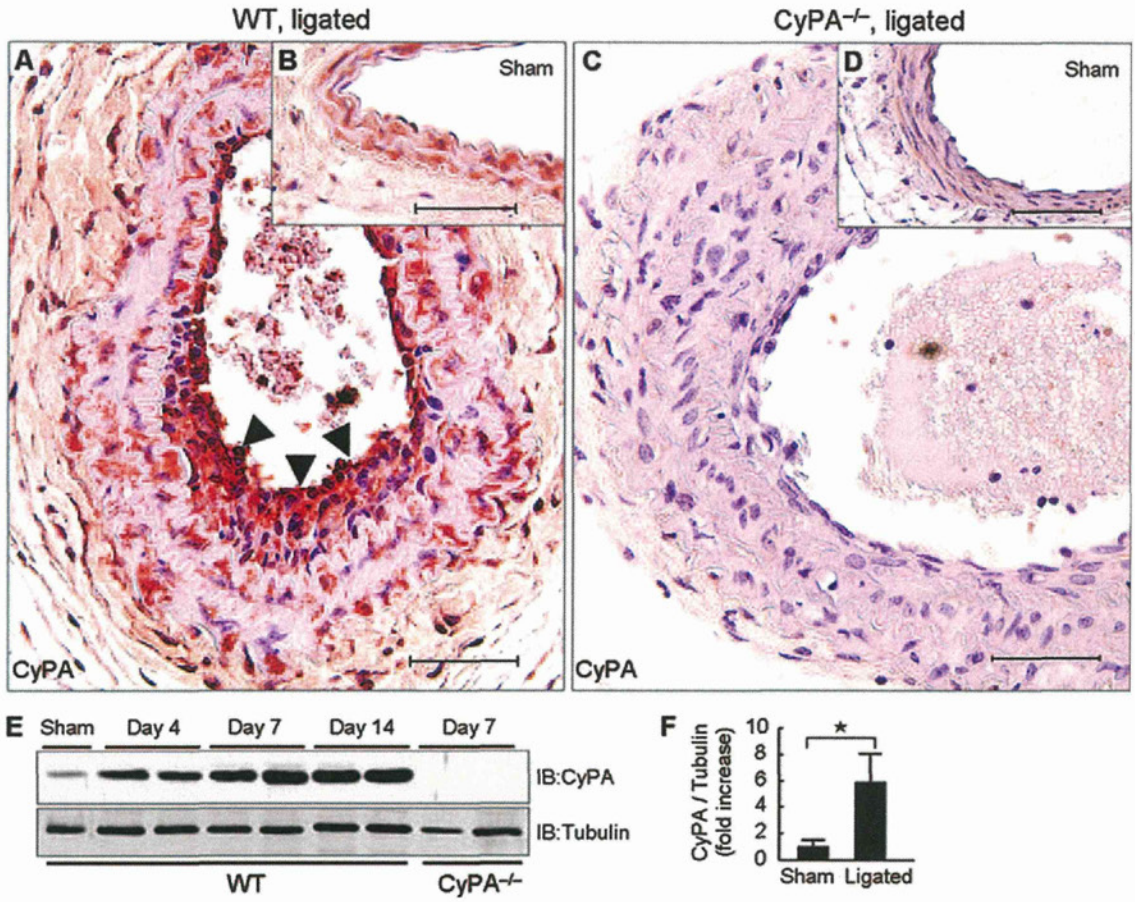

Figure 1. Carotid ligation enhances local CyPA expression. Representative immunostaining of CyPA in ligated (A and C) and sham (B and D) carotids from WT and CyPA$^{-/-}$ mice. Arrowheads show strong expression of CyPA in the intima. Scale bars=50 μm. E and F, Western blot analysis of CyPA in carotid homogenates of WT (n=8, solid bars) after ligation. Equal protein loading was confirmed with tubulin. Results are mean±SD. *P<0.01. IB indicates immunoblot.

Results

Vascular Remodeling After Carotid Ligation Was Significantly Reduced in CyPA$^{-/-}$ Mice

To test the hypothesis that CyPA contributes to vascular remodeling, we performed complete carotid ligation in WT and CyPA$^{-/-}$ mice. ROS generation and the proliferation of VSMCs play significant roles in intima formation in this model.[25,26] Immunostaining and Western blotting revealed that expression of CyPA increased after carotid ligation in WT mice, with highest expression in the intima (Figure 1A, arrows). In arteries that underwent a sham procedure, no increase in CyPA expression or intima formation was observed (Figure 1B). Quantification by Western blot showed a significant increase in CyPA expression after ligation in WT mice (Figure 1E and 1F). In CyPA$^{-/-}$ mice, there was no CyPA expression in either sham or ligated vessels (Figure 1C and 1D). These results indicate that blood flow cessation increases local CyPA expression. In sham WT and sham CyPA$^{-/-}$ controls, there was no intimal hyperplasia (Figure 2A and 2D), no differences in the thickness of elastic lamina (Figure 2B and 2E), similar α-SMA expression (Figure 2C and 2F), and no differences in medial area (Figure 2M, 2N, and 2O). The ligated arteries of WT mice (14 days) exhibited lumen narrowing (Figure 2G, 2H, and 2I), which was primarily a result of intimal hyperplasia and medial thickening. These changes were obviously reduced in CyPA$^{-/-}$ mice (Figure 2J, 2K, and 2L). Morphometric analysis of sham controls (Figure 2M, 2N, and 2O) showed no differences in intima, media, or intima/media (I/M) ratio in CyPA$^{-/-}$ mice versus WT mice. In contrast, analysis of ligated arteries on day 14 revealed that the intimal area was significantly smaller in CyPA$^{-/-}$ mice than in WT mice (Figure 2M). Additionally, we observed significantly increased medial thickening in WT mice compared with CyPA$^{-/-}$ mice (Figure 2N), which suggests that CyPA plays a crucial role in the development of vascular remodeling after blood flow cessation. Note that there was an increase in intimal area of CyPA$^{-/-}$ ligated vessels (Figure 2K and 2M) compared with sham, which indicates that other mechanisms also contribute to vascular remodeling. However, the I/M ratio of CyPA$^{-/-}$ mice was significantly less than that of WT mice (0.16±0.06 versus 0.29±0.13, P<0.01; Figure 2O), which indicates a crucial role of CyPA in vascular remodeling.

CyPA Induces VCAM-1 Expression and Promotes Inflammatory Cell Migration

An important initial step for the development of vascular lesions is inflammatory cell recruitment to the vascular wall.[7–9] Because CyPA induces VCAM-1 in human umbilical